Global Environmental Change 96 (2026) 103111

Contents lists available at ScienceDirect

Global Environmental Change

journal homepage: www.elsevier.com/locate/gloenvcha

# Combined benefits of multi-hazard early warnings on human mobility resilience to tropical cyclones

Haiyan Liu [a,b,c,*], Jianghao Wang [c,d,*], Zhifeng Cheng [b], Siqin Wang [e], Laurence Hawker [f], Jiatong Han [b], Phil J. Ashworth [g], Steve Darby [h], Faith Ka Shun Chan [i,j], Jian Liu [a], Andrew J. Tatem [b], Shengjie Lai [b,*]

[a] Ocean Data Center, Southern Marine Science and Engineering Guangdong Laboratory (Zhuhai), Zhuhai, Guangdong, China
[b] WorldPop, School of Geography and Environmental Science, University of Southampton, Southampton, UK
[c] State Key Laboratory of Resources and Environmental Information System, Institute of Geographic Sciences and Natural Resources Research, Chinese Academy of Sciences, Beijing, China
[d] University of Chinese Academy of Sciences, Beijing, China
[e] Spatial Sciences Institute, University of Southern California, Los Angeles, CA, USA
[f] School of Geographical Sciences, University of Bristol, Bristol, UK
[g] Department of Earth Science and Environmental Change, University of Illinois at Urbana-Champaign, Illinois, USA
[h] School of Geography and Environmental Science, University of Southampton, Southampton, UK
[i] School of Geographical Sciences, University of Nottingham Ningbo China, Ningbo, China
[j] Water@Leeds and School of Geography, University of Leeds, Leeds, UK

ARTICLE INFO

*Keywords:*
Early warnings
Tropical cyclone
Human mobility resilience
Climate adaptation
Disaster management

ABSTRACT

Multi-hazard early-warning systems (MHEWS) are critical for mitigating extreme weather impacts and enhancing disaster resilience. However, quantitative empirical evidence on how different types of early warnings individually and collectively trigger preventive actions and influence resilience remains limited. Here, using location-based human mobility data aggregated from over 1.1 billion mobile devices across Chinese cities, we quantified daily intracity human mobility responses to 21,126 early warning signals during 19 tropical cyclones (TCs) from 2021 to 2023. To represent disaster resilience under MHEWS protection, we developed a protected resilience index that integrates both the magnitude of mobility changes and recovery durations. We found that, compared with city-level TC warnings alone, combined multi-level, multi-hazard warnings resulted in a 52.4 % reduction in mobility during TC exposure days, thereby increasing avoided direct population exposure by around 57.1 %. Each additional warning type further shortened recovery times, collectively reducing recovery durations by at least 55.6 %, with larger effects observed for stronger TCs. Under MHEWS protection, protected resilience remained statistically similar between moderate-intensity TCs (34 kt and 50 kt) but declined significantly under severe (≥64 kt) conditions. Although absolute reductions in exposure were greater in high-frequency, coastal, and wealthier cities, relative improvements from MHEWS were more pronounced in less frequently affected, inland, and socioeconomically disadvantaged areas. Consequently, MHEWS significantly narrowed resilience disparities among cities facing equivalent hazard exposures. This study introduces a scalable, behaviour-based framework for quantifying early-warning effectiveness, highlighting the essential role of integrated multi-level and multi-hazard warnings in disaster preparedness across cities amid escalating climate risks.

## 1. Introduction

Tropical cyclones (TCs) are a leading cause of extreme weather-related fatalities and economic losses worldwide (WMO, 2021). From the 1970s to 2010s, TCs caused 779,324 deaths and $1.4 trillion in economic losses, accounting for 38 % of global natural disaster-related

* Corresponding authors at: Ocean Data Center, Southern Marine Science and Engineering Guangdong Laboratory (Zhuhai), Zhuhai, Guangdong, China.
*E-mail addresses:* liuhaiyan@whu.edu.cn, haiyan.liu@soton.ac.uk (H. Liu), wangjh@lreis.ac.cn (J. Wang), z.chen@soton.ac.uk (Z. Cheng), siqinwang@usc.edu (S. Wang), laurence.hawker@bristol.ac.uk (L. Hawker), j.han@soton.ac.uk (J. Han), philip10@illinois.edu (P.J. Ashworth), s.e.darby@soton.ac.uk (S. Darby), Faith.Chan@nottingham.edu.cn (F.K. Shun Chan), liujian@sml-zhuhai.cn (J. Liu), a.j.tatem@soton.ac.uk (A.J. Tatem), shengjie.lai@soton.ac.uk (S. Lai).

https://doi.org/10.1016/j.gloenvcha.2025.103111
Received 8 August 2025; Received in revised form 5 December 2025; Accepted 31 December 2025
Available online 7 January 2026
0959-3780/© 2026 Elsevier Ltd. All rights are reserved, including those for text and data mining, AI training, and similar technologies.

damages (WMO, 2021). TC risks stem from a combination of climate-related hazards (e.g., winds, rainfall), population and asset exposure, and vulnerabilities linked to inadequate preparedness and socioeconomic conditions (Peduzzi et al., 2012; IPCC, 2022). By 2050, over one billion people are expected to live in low-lying, TC-prone cities, underscoring the urgent need for robust adaptation and risk management strategies to mitigate these rising risks and improve resilience (IPCC, 2022; Jing et al., 2002; UNDRR, 2024).

Early warning systems (EWSs) are widely recognized as critical tools for disaster preparedness and resilience enhancement (Tennant & Gilmore, 2020; UNDRR, 2023; UNDRR, 2024). Effective EWSs function as integrated platforms for hazard monitoring, risk assessment, and timely forecast dissemination, enabling preemptive actions and mitigating disaster impacts (UNDRR, 2023; UNDRR, 2024). International frameworks, including the Sendai Framework and the United Nations Sustainable Development Goals (SDG 13, Target 13.1), explicitly advocate strengthening early warning capacities and improving disaster risk management practices globally (United Nations, 2015a; United Nations, 2015b)(United Nations, 2015b). Furthermore, the UN Secretary-General's recent "Early Warnings for All" initiative underscores the global ambition to implement universal EWS coverage by 2027 (UNDRR, 2023). Despite such global advocacy, however, the practical effectiveness of EWSs critically depends on their capacity to translate hazard alerts into prompt preventive actions at community and individual scales (Fundel et al., 2019; Fearnley, 2023). High-profile cases of inadequate responses to early warnings, such as the 2021 Zhengzhou flood in China (State Council Disaster Investigation Team of China, 2022) and the 2024 Hurricane Helene in the United States (Terrill, 2024), highlight ongoing challenges in bridging the gap between timely warnings and effective disaster prevention. Existing evaluations of EWS effectiveness have largely concentrated on technical forecast accuracy (Cremen et al., 2022) or on investigating the causes of warning ineffectiveness through interviews and social media analyses (Roy et al., 2015; Perera et al., 2020; Kitazawa & Hale, 2021; Yore & Walker, 2021), resulting in a notable gap between theoretical policy frameworks and empirically validated behavioural outcomes in large-scale settings (Fekete & Sandholz, 2021; Dittmer & Lorenz, 2024).

Areas frequently impacted by TCs often concurrently face secondary hazards such as torrential rainfall and flooding, suggesting potential added benefits from multi-hazard early-warning systems (MHEWS) compared to single-hazard systems (UNDRR, 2024). MHEWS integrates early warnings across multiple administrative levels (national, provincial, and city-level) and hazard types (e.g., TC wind, rainstorm warnings) (United Nations, 2015a), contrasting with traditional single-level, single-hazard warnings focused solely on wind impacts. Countries with high-frequency TC exposure, including the United States, China, and Japan, have adopted multi-level, multi-hazard warning frameworks, whereas other highly exposed nations, such as the Philippines, predominantly rely on single-hazard (e.g., wind-only) warnings issued at subnational scales. While MHEWSs theoretically promise greater effectiveness through coordinated institutional responses and enhanced preventive actions, they also require significantly greater institutional coordination, financial investment, and technical capacity, posing substantial implementation barriers for developing and least-developed countries (UNDRR, 2024). Yet, quantitative evaluations explicitly measuring the combined and added benefits of MHEWSs over single-hazard systems remain notably scarce.

Large-scale, location-based population mobility data provide unique opportunities for quantifying the effectiveness of MHEWSs, as they capture real-time, population-level behavioural responses to hazard alerts (Yabe et al., 2022; Liu et al., 2023a). Early warnings can prompt anticipatory actions such as evacuations, infrastructure protection, and activity suspensions, thereby reduce direct population exposure and accelerate recovery. Consequently, preemptive shelter-in-place or evacuation actions implemented before direct TC exposure represent measurable indicators of successful preventive actions (Hatchett et al., 2021). Prior studies have used mobility data to track post-disaster recovery trajectories by comparing changes relative to pre-event baselines, thereby reflecting the capacity of cities to maintain mobility and social stability under disaster stress (Lu et al., 2012; Wilson et al., 2016; Liu et al., 2023b). This mobility-based resilience framework has been widely applied in post-disaster studies in countries such as the United States (Acosta et al., 2020; Deng et al., 2021; Hong et al., 2021; Wang & Hu, 2024), China (Tang et al., 2023; Qian et al., 2024), Philippines (Abad and Fillone, 2020), and Bangladesh (Lu et al., 2016). Although various mobility data sources have been used, including official or international statistical reports, mobile signalling data from telecom operators, commercial datasets such as SafeGraph, and app-based data from technology companies such as Yahoo, these datasets consistently capture population movement during disasters (Yabe et al., 2020; Wilkinson et al., 2024). Comparative studies conducted in the United States and Japan (Yabe et al., 2020) as well as in Latin America and the Caribbean (Wilkinson et al., 2024) have revealed broadly consistent post-disaster mobility and recovery patterns, highlighting the universality of population response and return dynamics following large-scale disasters. However, most previous research has focused on impacts directly attributed to hazardous events themselves, without explicitly disentangling the distinct contribution of early warnings to reducing exposure and shaping resilience outcomes (Haque et al., 2012; Zhang and Li, 2022).

To address these critical knowledge gaps, this study used China, one of the countries most frequently impacted by TCs globally (Jing et al., 2002), as a large-scale empirical context. According to international disaster loss statistics (EM-DAT), between 2000 and 2024, China accounted for 31.1 % of the global population affected and 8.6 % of total adjusted economic losses associated with TCs (CRED, 2025). In 2024 alone, TCs caused direct economic losses of approximately US$11.9 billion dollars across the country, highlighting China's disproportionate exposure and disaster burden (Office of the National Disaster Reduction Committee & Ministry of Emergency Management, 2025). To mitigate this risk, China's disaster governance has undergone a paradigm shifted from reactive disaster response to proactive risk management as reflected in its national policy documents (State Council, 2022), with substantial investments in funding substantial upgrades to its MHEWS infrastructure from satellites to last-mile local alerts. Its MHEWS structure, characterized by hierarchical responsibility and territorial management, allows provincial and municipal authorities to issue distinct yet parallel warnings. This institutional arrangement provides an ideal empirical setting to quantify the combined effects of multi-level and multi-hazard early warnings on mobility-based resilience.

Leveraging daily city-level intracity mobility intensity data generated from real-time locations of more than 1.1 billion mobile devices from 2021 to 2023, we systematically assessed how populations responded to 21,126 early warnings (3,668 multi-level TC warnings and 17,458 city-level rainstorm warnings) across 19 TC events. This study had four specific objectives, aiming to: (1) quantify how different early warnings, varying by administrative level, hazard type, and intensity, reduce disaster direct exposure and accelerate post-disaster recovery; (2) evaluate the added benefits of MHEWS that combine multi-level and multi-hazard warnings compared to single-hazard warnings in modulating these dynamics; (3) assess the resulting mobility resilience capacity of cities under MHEWS coverage across varying hazard intensities; and (4) identify heterogeneity in these effects across cities with varying TC frequencies, geographic locations, and socioeconomic conditions. By providing explicit empirical evidence on these dynamics, our research quantifies the effectiveness of preemptive actions triggered by early warnings and offers policy-relevant insights to inform the design and optimization of MHEWS.

## 2. Conceptual framework

We developed a conceptual framework that delineates mobility

resilience to TCs into three interrelated concepts: inherent resilience, observed resilience, and protected resilience (Fig. 1). Inherent resilience refers to the capacity for collective mobility response and recovery in the complete absence of prior early warnings and related preparatory actions. Observed resilience captures the overall mobility dynamics throughout a TC event when MHEWS are in place. As MHEWS cannot fully eliminate disaster impacts, protected resilience represents the changes and recovery capacity of collective population mobility that still occurs under MHEWS protection. This may arise from direct exposure due to non-compliance with warning advice (Roy et al., 2015; Yore & Walker, 2021), or from indirect effects such as damage to local infrastructure that delays the resumption of intracity activity (Lu et al., 2012; Yabe et al., 2020). All three resilience indicators integrate both the magnitude and duration of mobility change, represented by the area between the pre-event baseline and the observed mobility curve, reflecting the extent to which communities can anticipate, absorb, adapt to, and recover from disruptions (Hong et al., 2021; IPCC, 2022). If a city were to experience a TC without any warnings, these three measures would theoretically converge. Under the actual coverage of MHEWS, warnings may initially reduce mobility, leading to lower observed resilience. However, unlike the mobility reductions caused by hazardous weather exposure, such reductions are deliberate and protective, effectively mitigating direct disaster exposure and likely enhancing protected resilience.

In China, owing to the widespread development and national wide coverage of MHEWS, inherent resilience is too rare to be statistically measurable. Therefore, we quantified the combined benefit of MHEWS, referring to the integration of multi-level and multi-hazard warnings, from three perspectives: a) Reducing direct disaster exposure, measured by the preemptive mobility reduction ratio, which captures the proportion of preemptive mobility decline associated with early warnings during the TC exposure period; b) Shortening recovery time, evaluated by comparing theoretical and observed recovery times (Fig. 1). Recovery time is defined as the period from hazard onset ($t$) to the first return of mobility to its baseline level ($t_2$). The theoretical recovery time is derived from the lag period of hazardous weather estimated by the model, representing the expected duration of the hazard's impact (from $t$ to $t_3$); c) Narrowing protected resilience gaps across TC intensity levels and socioeconomic contexts, where protected resilience is estimated as the difference between observed resilience and the mobility change associated with MHEWS (Fig. 1).

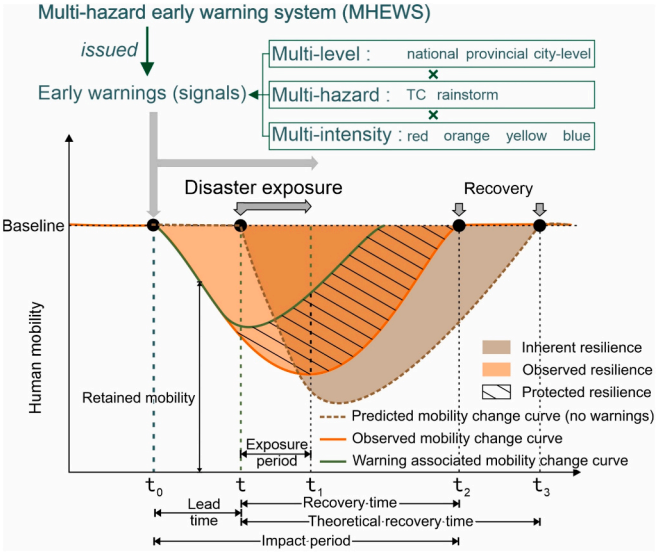



**Fig. 1. Conceptual framework of mobility changes under TCs and early warnings.** The horizontal grey arrows represent the coverage period of early warnings or disaster exposure.

## 3. Methods

### 3.1. Data collection and preprocessing

#### 3.1.1. Mobility data and recovery trajectories

Publicly available city-level daily intracity mobility intensity was obtained from Baidu's Qianxi data portal (https://qianxi.baidu.com/). This platform provides aggregated human mobility indices based on over 120 billion daily location-based service (LBS) queries collected from more than 1.1 billion mobile devices (Gibbs et al., 2020). Ethical clearance for collecting and using secondary data in this study was granted by the institutional review board of the University of Southampton (ERGO II 87924.A1). All data were supplied and analysed in an anonymous format, without access to personal identifying information. While we acknowledge the theoretical risk of reidentification when integrating multiple spatial datasets, this risk is minimal in our study due to the high level of spatial (prefectural-city level) and temporal (daily) aggregation of the mobility data. Intracity mobility intensity is defined as a standardized index representing the proportion of residents engaging in outdoor activities within a given city on each day, covering a total of 459 observational days from 2021 to 2023.

We calculated changes in mobility intensity relative to a pre-TC baseline to generate mobility change curves. The retained mobility ratio for each city on a given day was defined as:

$$M_{i,t} = \frac{MI_{i,t}}{B_{i,t}} \quad (1)$$

where $MI_{i,t}$ and $B_{i,t}$ represent the daily mobility intensity and baseline values for city $i$ on day $t$, respectively. The mobility reduction $MB_{i,t}$ was calculated as $1 - M_{i,t}$, with recovery considered complete once the ratio first exceeded 1 following TC exposure.

To establish the baseline, we used the average mobility from the week preceding the first national-level TC warning, as national warnings are typically issued earlier than regional or city-level alerts and are designed to prompt anticipatory behaviour. Because TCs occur frequently in China, with intervals between consecutive events sometimes shorter than a week, we selected one representative TC from each of three key periods, i.e., June, July and August (summer vacation for students), and September, ensuring at least 20 consecutive days without other TC events before each selection. Following standard practice in human mobility research (Hong et al., 2021; Google LLC, 2022), we adopted the mean mobility during the week before each TC's initial national warning as the reference baseline (Supplementary Table S1), and excluded public holidays to avoid bias from abnormal mobility patterns. In the sensitivity analysis, we compared outcomes under different baseline definitions (Supplementary Fig. S1) and evaluated model fits across these baselines (Supplementary Table S2) to confirm the robustness of results and justify the adoption of a multi-baseline approach. Given the relatively short study period (spanning within two months post-baseline), we did not adjust for seasonal variations in mobility intensity (Liu et al., 2023b).

#### 3.1.2. TC data and wind field modelling

TC track data used in this study were obtained from the China Meteorological Administration (CMA) (http://typhoon.nmc.cn/web.html). CMA served as one of the data sources for the International Best Track Archive for Climate Stewardship (IBTRACS) database. Unlike IBTRACS, which retained data at three-hour intervals, CMA provided data at hourly intervals, offering a higher temporal resolution for more detailed analysis. The dataset includes latitude and longitude positions, maximum sustained wind speeds at 10 m above sea level, central pressure, and quadrant radii for 34 kt, 50 kt, and 64 kt wind thresholds (R34, R50, R64) before landfall, segmented by quadrants (Feng et al., 2014). We excluded storm observations with maximum wind speeds below 34 kt.

To delineate areas exposed to different intensities of TCs, we used two approaches in wind field modelling. The first was the "radii and track" approach based on quadrant-specific CMA data. Before landfall, we accounted for the asymmetrical wind field of TCs by using quadrant-specific wind profiles (R34, R50, R64) to determine exposure areas under each wind intensity as TCs approached. After landfall, all cities along the TC's track were considered affected, with exposure intensity determined by the maximum central wind speed. The second approach applied the Holland model to estimate the full wind field (Holland et al., 2010), dynamically calculating parameters like the radius of maximum wind (*Rmax*) (Chavas & Knaff, 2022) and the air pressure profile parameter (*B*) (Lin & Chavas, 2012). Peripheral pressures and air density were assigned based on commonly used values in Chinese TC studies: 1010 hPa and 1.2 kg/m$^3$, respectively (Holland, 1980; Xiao et al., 2011). This approach allowed calculation of wind speeds at various distances from the TC centre, identifying exposure regions for 34 kt (63–88 km/h), 50 kt (89–117 km/h), 64 kt (118–149 km/h), 80 kt (150–183 km/h), and 100 kt (>183 km/h) wind speeds.

Hourly exposure areas were aggregated into daily exposure regions, meaning a city could be exposed to multiple TC intensities within a single day. To account for the variation in TC impacts across city areas, we used WorldPop's 100 m-resolution population data in 2020 to estimate the proportion of the population exposed to each wind intensity (Stevens et al., 2015). Among the 368 administrative divisions with Baidu human mobility data, we found 110 cities directly exposed to TC winds exceeding 34 kt (Fig. 2a). Given that TC-induced rainfall can affect much wider areas than direct wind exposure, our analysis also included the provinces containing these directly affected cities and their neighbouring regions, encompassing 184 prefectural-level cities (administrative level 2) across 12 provinces.

Our analysis focused on the TC seasons from June to October during 2021–2023, a period marked by 19 TCs affecting China (Supplementary Table S1). Analysis of TC exposure data from 2004 to 2023 indicated that the 2021–2023 period was representative of long-term TC impacts, with city exposure proportions in these years aligning closely with observations from the previous two decades (Supplementary Fig. S2).

### 3.1.3. Early warning data collection and preprocessing

All disaster-related early warning signals during the TC-prone seasons were sourced from three channels: 1) the National Emergency Broadcast by China Media Group (http://www.cneb.gov.cn/), 2) official multi-channel network (MCN) accounts of the China National Early Warning Information Release Center (https://author.baidu.com/home?from=bjh_article&app_id=1641370415653479), and 3) the official Weibo accounts of local meteorological bureaus. These sources comprehensively captured the dissemination of early warnings across broadcast, multimedia platforms, and social networks. Where no warnings were reported through these channels, we assumed the signals were not successfully communicated. Each record included issuing authority (national, provincial, city, or district level), hazard type (TC or rainstorm), warning intensity (blue, yellow, orange, red), release time, and signal type (issued, updated, lifted). Due to the infrequent issuance of provincial or national-level rainstorm warnings, these were excluded from the analysis. After de-duplication, we identified 21,126 TC- and rainstorm-related warnings over the study period (Figs. 2b-2c).

For alignment with the spatiotemporal resolution of human mobility data, early warning data were adjusted both spatially and temporally. Spatially, warnings were aggregated at the city level; a city was considered warned if any district within its boundaries issued a signal. This adjustment reduced the spatial resolution of rainstorm warnings, typically issued at district or county levels, while TC warnings were generally city-level or above. Temporally, hourly warning data were translated to a daily scale: if a warning was lifted before 8 A.M. (prior to standard work and school hours), that day was considered warning-free. Conversely, warnings issued after 5P.M. were rolled over from the previous day's latest warning level. For multiple warnings issued between 8 A.M. and 5P.M., we recorded the highest intensity as the daily warning level. Temporal and spatial adjustments were applied to city-level warnings, while only temporal adjustments were made for provincial and national warnings. All data, particularly instances involving

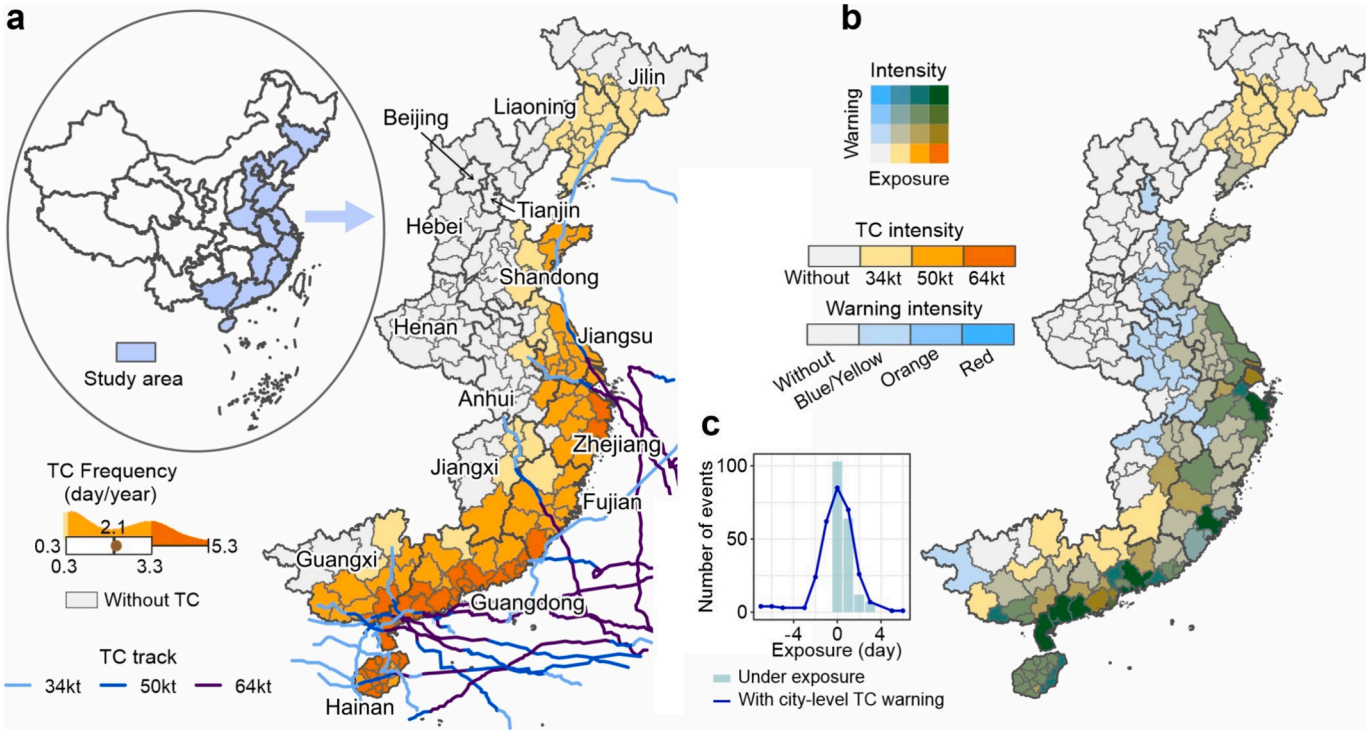



**Fig. 2. Spatial and temporal characteristics of TC impacts and early warning issuance across China. a**, TC tracks affecting China and annual days of exposure from 2021 to 2023. **b**, Temporal differences between TC exposure and city-level TC warning issuance. **c**, Spatial variations in the average highest TC exposure intensity and the corresponding average city-level TC warning intensities across cities.

TC exposure without corresponding city-level TC warnings, underwent manual verification to ensure completeness and accuracy.

#### 3.1.4. Other covariates

City administrative boundaries were accessed via the Amap API (https://datav.aliyun.com/portal/), which was approved by Chinese authorities. Daily reanalysed meteorological data, including wind speed (10 m u-component and v-component) and total precipitation from 2021 to 2023 at a 0.1-degree spatial resolution, were sourced from ERA-5 Land (Hersbach et al., 2020). These data were averaged daily for each city in Google Earth Engine (GEE), with wind speed calculated by combining the u and v components. Unconstrained version population distribution data for 2020 at a 100 m resolution were obtained from WorldPop, while city-level per capita GDP data at the end of 2020 were gathered from provincial and city statistical yearbooks. Public holiday periods for each year were retrieved from the official website of the General Office of the State Council of China (Lai et al., 2022). Daily policy stringency index, used as an indicator for non-pharmaceutical interventions (NPIs) during the COVID-19 pandemic in 2021 and 2022, was derived from the Oxford COVID-19 Government Response Tracker (Hale et al., 2021).

### 3.2. Model development and validation

Because TC exposure and warning issuance vary across space and time (Fig. 2), we developed spatiotemporal Bayesian hierarchical models to disentangle the average effects of early warnings and hazardous weather conditions on human mobility. Through their hierarchical structure, these models enable information sharing across cities and leverage spatiotemporal variations to estimate the average effect of each specific type of early warning (Banerjee et al., 2014).

The base model, constructed within the spatiotemporal Bayesian hierarchical framework, controlled for potential confounders influencing mobility changes at the city level relative to pre-TC baselines, including day-of-the-week effects, holidays, population size, spatial dependencies, and city-level heterogeneity. The model is as follows:

$$M_{i,t} = \alpha + \beta_{c(i)d(t)} + U_{c(i)w(t)} + S_{c(i)} + Vh + Vp_i \quad (2)$$

here, $\beta_{c(i)d(t)}$ represents the city-level day-of-the-week random effect, modelled using a cyclic first-order random walk (RW1) to account for the dependency of daily mobility changes on the preceding day. The second spatiotemporal random effect is captured by a modified Besag-York-Mollie (BYM) model, represented by the combination of $U_{c(i)w(t)}$ and $S_{c(i)}$. $U_{c(i)w(i)}$ addresses city-specific noise (e.g., governance capacity and policy implementation) through an unstructured spatial random effect at the city level, while $S_{c(i)}$ models the geographical and social spillover effects among cities through a conditional autoregressive term. The effectiveness of these two spatiotemporal random effects in capturing daily mobility changes has been demonstrated in previous analyses (Liu et al., 2023b). Both holiday $Vh$ and the total population size $Vp_i$ are included as fixed effects to control for their influence on mobility. The mobility changes were modelled as following a Gaussian distribution $M_{i,t}$ $N(\mu_{i,t}, \sigma^2)$, where $\mu_{i,t}$ was the expected mean and $\sigma$ was the standard deviation. Poisson and negative binomial models were also tested as potential baselines but were inadequate in addressing residual overdispersion in the spatiotemporal random effects. Fixed-effect coefficients were assigned regularising Gaussian priors with a mean of 0 and a precision of 1 (variance = 1) (Lowe et al., 2021). All random components, including day-of-week, week-index, city-level and province-level effects, as well as the Gaussian likelihood precision, were specified with Penalised Complexity (PC) priors defined as param = c (1, 0.01), implying a 1 % prior probability that the standard deviation exceeds 1 (Simpson et al., 2017). Model parameters were estimated using Integrated Nested Laplace Approximations (INLA) within a Bayesian framework (Blangiardo et al., 2013), carried out in R version 4.1.3.

Building on the base model, we incorporated key hazardous weather indicators, including daily average wind speed, total precipitation, and TC exposure ratio (i.e., the proportion of the population exposed to different TC intensity categories). TC warnings were categorized by administrative level (national, provincial, and city) and intensity, while rainfall warnings were assessed at the city level. Given that China's coastal defences and infrastructure have largely mitigated the impacts of storm surges (Ding et al., 2024), storm surge conditions and related warnings were not included in the analysis. DLNMs were applied to assess the non-linear and lagged impact of hazardous weather conditions (wind and precipitation) and early warnings on mobility changes (Gasparrini et al., 2010), simultaneously capturing the non-linear exposure–response relationships and the distributed timing of their effects. This method has been widely applied in studies examining the effects of climate and disaster on human health (Huang et al., 2023; Fletcher et al., 2025), enabling the estimation of both the intensity and temporal evolution of how early warnings and hazardous weather influence mobility. Natural cubic splines with three degrees of freedom were used for both the exposure and lag dimensions. For the exposure dimension, two internal knots were placed at equally spaced quantiles of each predictor. For the lag dimension, early-warning effects were evaluated over a 7-day window, whereas TC exposure ratios, average wind speed and precipitation were assessed over 14- or 21-day lag windows depending on the variable. Lag splines were defined with a single internal knot positioned at the midpoint of each lag period. The comprehensive model was defined as follows:

$$\begin{aligned} M_{i,t} = {} & \alpha + \beta_{c(i)d(t)} + U_{c(i)w(t)} + S_{c(i)} + Vh + Vp_i + f.l(ws,d)_i \\ & + f.l(prec,d)_i + f.l(R_{34},d)_i + f.l(R_{50},d)_i + f.l(R_{64},d)_i \\ & + f.l(W_{nt},d)_i + f.l(W_{pt},d)_i + f.l(W_{ct},d)_i + f.l(W_{cp},d)_i \end{aligned} \quad (3)$$

where $f.l(ws,d)_i$,$f.l(prec,d)_i$, $f.l(R_{34},d)_i$, $f.l(R_{50},d)_i$, $f.l(R_{64},d)_i$, $f.l(W_{nt},d)_i$, $f.l(W_{pt},d)_i$, $f.l(W_{ct},d)_i$, $f.l(W_{cp},d)_i$ represent the DLNMs for average wind speed, precipitation, 34 kt TC exposure ratio, 50 kt TC exposure ratio, 64 kt or above TC exposure ratio, national TC warnings, provincial TC warnings, city-level TC warnings, and city-level rainstorm warnings, respectively. In the experiments using Holland wind field data, the DLNMs also included population exposure ratios for 80 kt and 100 kt or above wind speeds. Average wind speed, precipitation, and NPI stringencies in 2021 and 2022 were calculated as deviations from baseline averages. Considering the influence of COVID-19 interventions in 2021 and 2022, primary results were derived from 2023 data, with earlier years incorporated into sensitivity analyses.

All factors were first examined for multicollinearity using Pearson correlation test. When two variables were highly correlated ($r > 0.05$), only the one with the stronger association with the outcome variable was retained in the model (results in Supplementary Fig. S3 and S4). The data obtained from the two wind field calculation methods were highly correlated, with the Holland model data exhibiting higher autocorrelation. Therefore, we based the main analysis on the "radii and track" population exposure ratios, while using the Holland model for sensitivity analysis.

To identify the best-fitting model, we compared model performances using Deviance Information Criterion (DIC) and log score (Lowe et al., 2021). The DIC balances model accuracy with complexity by estimating the effective number of parameters, while the log score assesses predictive power through leave-one-out cross-validation. For both criteria, lower values indicate a better fit. We conducted residual diagnostics to assess model adequacy. To validate the improvements provided by data-driven models, we also assessed the difference in mean absolute error between the base models and the selected models, determining the proportion and locations of cities where the model fit had improved.

We treated early warnings of different administrative levels and hazard types as independent events because China's MHEWS operates under the principle of hierarchical responsibility and territorial

management (State Council, 2022). Specifically, national-level warnings are issued by the CMA to provide nationwide situational awareness but do not directly trigger or determine the timing of provincial or municipal warnings. Local governments are authorised to develop, issue, and update their own warnings based on real-time local conditions and impact assessments. Therefore, in the Chinese context, treating warnings at different levels and hazard types as independent but potentially concurrent information sources accurately reflects how the system functions in practice. Even so, we conducted sensitivity analyses to explore potential interaction effects. Specifically, we examined whether concurrent national- or provincial-level warnings influenced the effectiveness of city-level TC warnings, whether the early issuance of TC warnings affected the effectiveness of subsequent rainstorm warnings, and whether the same type of TC warning produced different effects under varying TC intensities.

### 3.3. Assessing impacts of early warnings on mobility resilience

#### 3.3.1. Avoided exposure

Assuming that exposure to warnings and hazardous weather conditions is associated with human mobility reduction, we assessed the potential mobility reduction *MB* under exposure compared to non-exposure as:

$$MR = 1 - RR \text{ and } RR = \frac{P(R|E)}{P(R|\neg E)} \tag{4}$$

here, $P(R|E)$ is the posterior ratio of retained mobility under exposure and $P(R|\neg E)$ represents the prior ratio under baseline conditions (baseline being 100 %). Thus, *RR* gives the average retained mobility. We analysed *MR* and its 95 % credible intervals over lag periods, considering cases where exposure led to a mobility reduction (i.e., $MR > 0$). Since impacts could persist for several days, the impact period (lag days) for each factor was defined as days with $MR > 0$. Although incorporating average city wind speed improved model fit, it did not significantly affect *MR* (Supplementary Table S3 and Fig. S5) and was therefore treated solely as a control variable without further mention.

Because we assumed that all warnings and hazardous weather events independently affect population mobility, we calculated their combined effect when occurring simultaneously based on the joint probability of independent events. The preemptive mobility reduction ratio (abbreviated as preemptive reduction ratio) during the TC exposure period was calculated as:

$$PR_{w,it} = \frac{\overline{MR}_{w,it}}{1 - \overline{M}_{W,it} \times \overline{M}_{H,it}} = \frac{1 - \overline{M}_{w,it}}{1 - \prod\overline{M}_{w,it} \times \prod\overline{M}_{hw,it}} \tag{5}$$

$$Leadn_PR_{w,it} = \frac{Leadn_\overline{MR}_{w,it}}{1 - Leadn_\overline{M}_{W,it} \times \overline{Leadn_M}_{H,it}} \tag{6}$$

$$Leadn_\overline{MR}_{w,it} = 1 - \prod_{0}^{n}\overline{M}_{w,i(t-n)} \tag{7}$$

here, $PR_{w,it}$ denotes the preemptive reduction ratio of a specific warning *w* issued by unit *i* at exposure time *t*, $1 - \overline{M}_{W,it} \times \overline{M}_{H,it}$ representing the maximum mobility reduction ratio under the combined effects of all warnings and hazardous weather. $Leadn_\overline{MR}_{w,it}$ is the preemptive reduction ratio of warnings *w* issued n times prior to the exposure time, accounting for both the direct impact of warnings issued at time *t* and the lingering effects of historical warnings that persist over previous periods.

The preemptive reduction ratio quantifies, for each city and TC event, the proportion of direct exposure reduction attributable to early warnings during the TC exposure period. We further estimated the aggregate and regional differences in avoided exposure by incorporating city-level population size and baseline mobility intensity. The corresponding formulas are presented below:

$$E2_{i,t} = E1_{i,t} \times (B_{i,t}/10) \tag{8}$$

$$AE1_{i,t} = E2_{i,t} \times MB_{i,t} \tag{9}$$

$$AE2_{i,t} = AE1_{i,t} \times Lead3_\overline{MR}_{W,it} \tag{10}$$

here,$E1_{i,t}$ denotes the estimated static exposure population in city *i* on TC exposure day *t*, calculated by overlaying the wind field with WorldPop population distribution data. One person exposed to one typhoon day is counted as one population-day of exposure. $E2_{i,t}$ represents the population actually at risk due to outdoor activity on day *t* in city *i*, estimated as the product of $E1_{i,t}$ and the baseline intracity mobility level $B_{i,t}$. Although the intracity mobility index is standardized, it has been shown to correlate positively with actual mobility volumes (Zhao & Gao, 2024). During the 2023 study period, the average intracity mobility index across mainland China was $6.66 \pm 1.10$. For comparison, Meta movement distribution data indicated that the daily proportion of residents travelling from home locations (i.e., distance $> 0$ km) in similarly dense and transit-oriented regions was 59.2 % $\pm$ 5.1 % in Japan, 61.0 % $\pm$ 2.2 % in South Korea, 64.1 % $\pm$ 1.4 % in Singapore, and 63.8 % $\pm$ 1.7 % in Hong Kong, respectively (Meta, 2025). Because no equivalent datasets exist for Chinese cities, we approximated $B_{i,t}/10$ as the daily proportion of residents engaging in outdoor activity.

$AE1_{i,t}$ represents the total reduction in exposure due to decreased intracity mobility on day *t*, or the total avoided direct exposure. $AE2_{i,t}$ represents the reduction in direct exposure resulting from preemptive actions associated with early warnings. Given that the intracity mobility index-based proportion involves unavoidable measurement uncertainties, our estimates should be interpreted as the order of magnitude of avoided exposure associated with early warnings, rather than as an exact count of avoided population-days.

#### 3.3.2. Shortened recovery time

To assess the impact of early warnings on post-disaster recovery time, we treated the model-estimated lag period of TC exposure as the theoretical recovery time. This value represents the expected duration of hazard impacts in the absence of warning and preparedness. We then compared it with the average observed recovery time, and the difference was interpreted as the benefit provided by early warnings. To ensure a cautious interpretation, cities were categorised according to the maximum TC intensity experienced during each event, allowing us to differentiate the effects of early warnings under varying hazard severities. It should be noted that the model-estimated lag period does not represent conditions of complete absence of MHEWS, and therefore the estimated reduction in recovery time is a probably underestimated estimate.

#### 3.3.3. Mobility resilience

Still based on the joint probability of independent events, we calculated the overall preemptive reduction ratio of early warnings during the impact period during TC events as:

$$W = \frac{\int_{t_0}^{t_2}\overline{CMR}_W dt}{\int_{t_0}^{t_2}\overline{CMR} dt} \tag{11}$$

here, the impact period refers to the duration from the issuance of the first early warning during the event to the first time mobility returns to its baseline level (from $t_0$ to $t_2$ in Fig. 1). $\overline{CMR}$ represents the cumulative reduction in intracity mobility caused by both hazardous weather and early warnings over their respective lag periods; $\overline{CMR}_W$ denotes the cumulative mobility reduction attributable solely to early warnings over their lag periods.

By eliminating the mobility changes induced by warnings, the protected resilience should be:

$$PR = (-1) \times \int_{t_0}^{t_2} MR_{i,t}dt \times (1 - W) \quad (12)$$

Compared with the commonly used observed resilience $OR = (-1) \times \int_{t_0}^{t_2} MR_{i,t}dt$, this metric $PR$ excludes the mobility changes triggered by early warnings during this time. Because $MR_{i,t}$ represents the reductions in intracity mobility, observed resilience and protected resilience are expressed as dimensionless negative quantities. Accordingly, larger (i.e., less negative or closer to zero) values indicate higher resilience, reflecting a greater ability to maintain baseline activity levels under hazard exposure.

It should be noted that temporally consecutive TC events may lead to compounded impacts and delayed post-disaster recovery, thereby biasing the estimation of early-warning effects. To mitigate this potential bias, consecutive TC events were excluded from the analysis. Specifically, if a city was affected by two TCs within a 10-day interval, data from both events were removed from the quantification of early-warning impacts.

#### 3.3.4. Significance testing of group differences

To highlight the differential benefits of various warning types and combined warnings, we compared the distribution of outcomes across different TC intensity levels. We employed the Wilcoxon rank-sum test (W-test) to assess whether group differences were statistically significant. A p-value below 0.05 was considered indicative of statistical significance. For avoided exposure, calculations were conducted at the daily level, with TC intensity defined as the maximum TC intensity experienced by the city on each TC exposure day. In contrast, recovery time and protected resilience were analysed at the event level, where a "TC event" is defined as a single instance of a city being affected by a specific TC. TC intensity in this context was defined as the maximum TC intensity experienced by the city during the entire TC event period.

### 3.4. Heterogeneity analysis

To determine whether the effect of early warnings in narrowing protected resilience gaps varied across urban settings, we categorised cities by TC exposure frequency, geographic location, and socioeconomic conditions. Cities with total exposure days across the three-year study and in 2023 above the median were classified as high-frequency cities (n = 28), while those below the median but still exposed were considered low-frequency cities (n = 16). Coastal cities were defined as those within 50 km of the coastline (n = 62), and the rest as inland cities (n = 122). Wealthier cities, with 2020 GDP per capita in the top 30 % percentile, comprised 55 cities, while the bottom 30 % defined the 54 less affluent cities. The analyses were conducted separately for each category, allowing for comparison across groups.

## 4. Results

### 4.1. Mobility disruptions under TC exposure

In general, TCs led to substantial reductions in intracity mobility across 110 exposed Chinese cities from 2021 to 2023, with an average of 2.1 days of exposure per year (Fig. 2a). The first day for a city impacted by TC winds exceeding 34 knots (kt for short) in each TC was designated as the "Day 0" of exposure, and a single TC typically affected cities for approximately two days (Fig. 2b). Consequently, the average mobility reduction peaked on Day 1 after exposure, with mobility returning to pre-TC baseline levels by Day 8 if no consecutive TCs occurred (Fig. 3a). The magnitude of mobility reduction was proportional to TC intensity (measured in TC Wind, kt), with reductions of 8.4 % ± 11.5 % at 34 kt (tropical storms), 13.5 % ± 7.7 % at 50 kt (strong tropical storms), and 24.3 % ± 19.1 % at 64 kt or above (typhoons, severe typhoons, and super typhoons) (Fig. 3b). The observed reduction likely indicates that individuals either relocated or sheltered indoors, thus avoiding their direct exposure to the TCs.

Notably, the decline in intracity mobility began two days before Day 0, aligning with the issuance of city-level TC warnings (Fig. 2b and Fig. 3c). While regulations in China specify the required warning intensity (i.e., blue, yellow, orange, and red, increasing with severity) based on TC intensity (see Appendix Table A1), the warnings issued did not always align with the observed TC intensities (Figs. 2b-2c). Higher warning intensities were associated with greater mobility reductions, with the maximum reductions of 5.4 % ± 4.0 % for blue warnings, 11.1 % ± 6.2 % for yellow, 11.5 % ± 11.9 % for orange, and 26.5 % ± 21.5 % for red warnings (Fig. 3c). Cities without any city-level TC warnings experienced greater mobility reductions and slower recovery than those with even a slight (blue) warning. This suggests that early warnings might positively influence both the timing and magnitude of mobility recovery.

### 4.2. Combined benefits in reducing exposure

We disentangled daily intracity mobility changes induced by early warnings from those driven by hazardous weather during TCs using spatiotemporal Bayesian hierarchical models combined with DLNMs. We found that incorporating hazardous weather and early warnings into the DLNM framework significantly improved explanatory power compared to linear models, as evidenced by DIC values and log-likelihood scores. The formulas and results of all 23 comparative models are detailed in Supplementary Table S3. The comprehensive

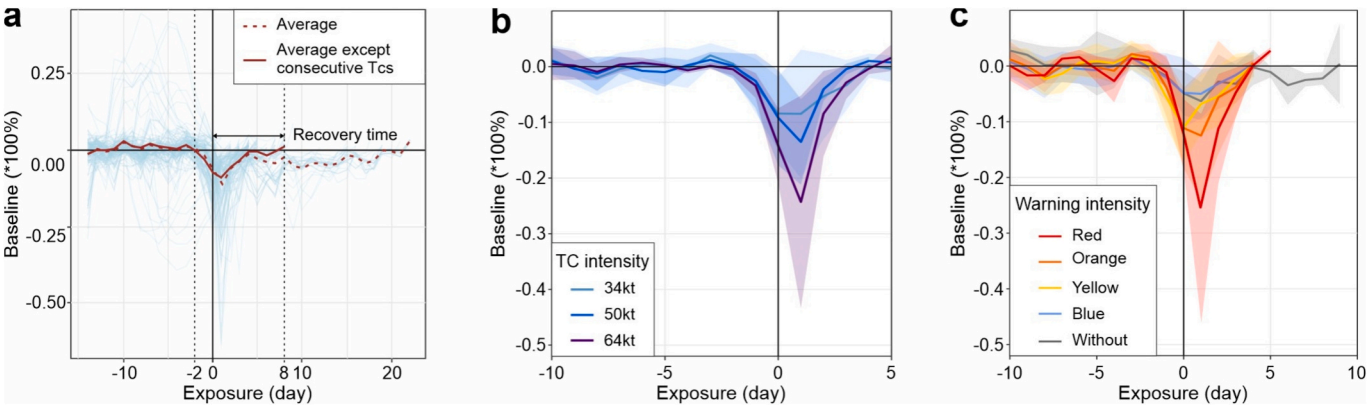



**Fig. 3. Observed mobility change curves under TC impacts. a**, Average intracity mobility changes across cities with TC exposure relative to baseline, with each light blue line representing one city during one TC event; **b**, Average intracity mobility changes under different TC exposure intensities; **c**, Average intracity mobility changes under different city-level TC warning intensities. The shaded areas in **b** and **c** indicate one standard deviation (SD). (For interpretation of the references to colour in this figure legend, the reader is referred to the web version of this article.)

model, integrating the DLNMs of all weather and warning factors, demonstrated the best overall fit, improving the mean absolute error in 94.6 % of cities relative to the base model (Supplementary Fig. S6). Residuals were centred around zero with no systematic trends or spatial clustering, indicating no heteroscedasticity or misspecification and confirming that the model effectively captured the spatiotemporal structure of the data (Supplementary Fig. S7). Notably, while the inclusion of city-level average wind speed enhanced model fitness, it did not significantly reduce mobility (Supplementary Fig. S5). In contrast, rainfall, TC exposure, and associated warnings were strongly associated with substantial reductions in intracity mobility intensity (Supplementary Fig. S8-S9).

Fig. 4a illustrates the issue-response relationship between different types of warnings and mobility changes. We found that more localized and higher-intensity warnings were particularly effective at triggering indoor risk-avoidance behaviours. Specifically, red city-level TC warnings were associated with a 12.3 % reduction in intracity mobility on the day of issuance (95 % CI: 11.0 %–13.6 %), while orange, yellow, and blue warnings were associated with reductions of 5.4 % (95 % CI: 4.7 %–6.2 %), 1.8 % (95 % CI: 1.3 %–2.4 %), and 0.8 % (95 % CI: 0.4 %–1.2 %), respectively. Higher-level administrative warnings had broader coverage but smaller impacts: red provincial TC warnings were associated with a maximum 9.6 % reduction (95 % CI: 7.7 %–11.4 %), while blue warnings showed a minimal 0.3 % reduction (95 % CI: 0–0.5 %). National-level red warnings reduced mobility by a maximum of 1.8 % (95 % CI: 1.6 %–2.0 %), with blue warnings showing no measurable effect. City-level rainstorm warnings had the largest reduction of 3.4 % (95 % CI: 2.9 %–3.8 %) for red warnings, while blue, yellow, and orange warnings all produced similar reductions of around 1.4 %.

Over half of the intracity mobility reduction on TC exposure days was associated with preemptive avoidance triggered by early warnings. Same-day warnings were associated with a preemptive reduction ratio of 48.2 % (interquartile range [IQR]: 29.5 %–62.8 %) (Fig. 4b). Recognizing that warnings might exert lagged effects, i.e., mobility changes observed on TC exposure days could be influenced by warnings issued several days earlier, we incorporated lagged effects from warnings issued up to three days prior to TC exposure (Fig. 4c), which increased the preemptive reduction ratio across all warnings to 52.4 % (IQR: 33.1 %–66.9 %) (Fig. 4d). After accounting for differences in baseline mobility levels and population sizes across cities (Supplementary Fig. S10), approximately 75.4 million population-days in 2023 avoided direct TC exposure through shelter-in-place actions during TC events, of which 41.0 million person-days (54.4 %) were directly associated with early warnings (Fig. 4e). While changes in intracity mobility intensity captured only the number of individuals fully avoiding outdoor activities on a given day, without accounting for vulnerable groups trapped or adversely affected while sheltering in place, it nonetheless offers a robust estimate of the population-level exposure reductions achieved through early warnings.

To assess the added benefit of MHEWSs relative to single-hazard EWSs, we compared the combined population exposure reductions from multi-level, multi-hazard warnings against those from city-level TC

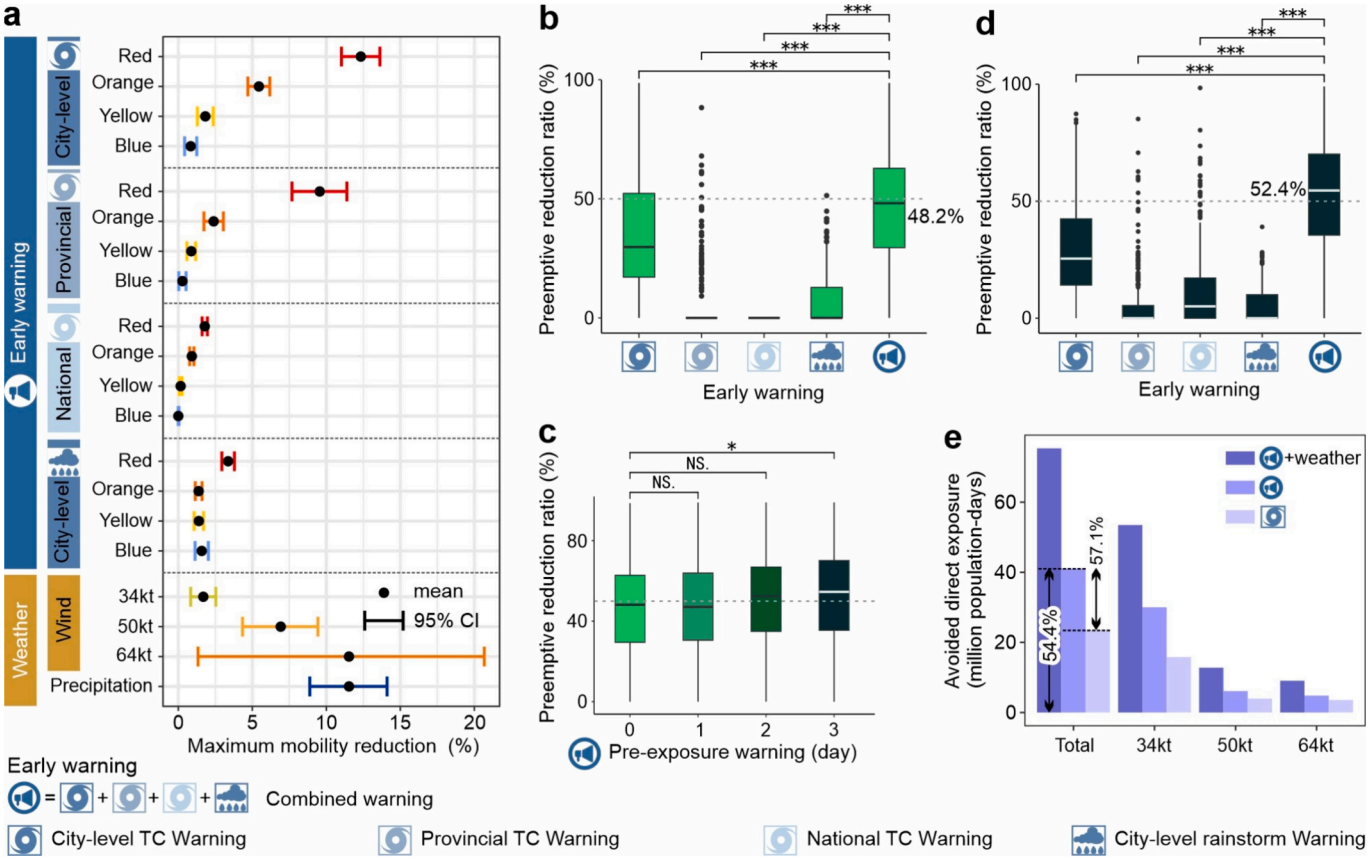



**Fig. 4. Impacts of early warnings on intracity mobility reduction during TC exposure. a**, Maximum mobility reduction and its 95 % confidence interval (CI) of intracity mobility under different warnings and hazardous weather conditions; **b, d**, Preemptive reduction ratios for various warning types on TC exposure days, shown without accounting for lag effects (**b**) and after incorporating lagged responses triggered by warnings issued with a 3-day lead time before TC exposure (**d**); **c**, Preemptive reduction ratios for the combined effect of all warning types on TC exposure days, accounting for lagged responses from warnings issued at varying lead times; **e**, Total number of people staying at home due to reduced intracity activities, representing the avoided direct population exposures to TCs. In each box in **b-d**, the central line represents the median, the edges of the box correspond to the first and third quartiles, and the whiskers extend to the minimum and maximum values. Significance levels were determined using two-sided Wilcoxon tests (*** $P < 0.001$; ** $P < 0.01$; * $P < 0.05$; NS, $P > 0.05$).

warnings. City-level TC warnings represent the most common form of single-hazard EWS during TCs in many countries, making them an appropriate baseline for comparative analysis. Relative to the 23.4 million person-days of avoided direct exposure associated with city-level TC warnings, MHEWSs increased the avoided exposure by 57.1 % (Fig. 4e). Although this percentage declined slightly with increasing TC intensity, because cities under more severe conditions would issue higher-intensity city-level warnings and implement stricter protective measures, the added benefit of MHEWSs remained substantial. Across all TC intensity levels, MHEWSs consistently achieved over 40 % greater avoided direct exposure compared to single-hazard EWSs (Fig. 4e), underscoring their superior protective capacity.

### 4.3. *Early-warning effects on recovery and protected resilience under TCs*

Having established the role of early warnings in reducing exposure, we next examined whether they also contributed to shortening the recovery time following TC impacts. We used the mean impact period (i.e., lag days) of hazardous weather impacts on mobility as a proxy for theoretical post-disaster recovery time and found that hazardous weather exerted longer effects than early warnings (Fig. 5a). Rainstorms affected mobility for up to 5 days, while TC impacts persisted beyond 9 days (Supplementary Fig. S9). Higher TC intensities further extended lag durations, with impacts lasting up to 9, 13, and 21 days under 34 kt, 50 kt, and 64 kt or above exposures, respectively. In contrast, city-level warnings, whether for TCs or rainstorms and regardless of intensity, affected mobility for only 2 days, while provincial and national warnings extended up to 7 days (Supplementary Fig. S8).

Controlling for TC exposure intensity, the combination of multiple early warning types was associated with accelerated recovery (Fig. 5b). Under 34 kt TCs, average observed recovery occurred on Day 9 without city-level TC warnings, Day 8 with city-level TC warnings, and remained on Day 8 when both city- and provincial-level TC warnings were issued. However, when all warning types were present, recovery time further shortened to Day 4 (Fig. 5b, Supplementary Fig. S11). Under 50 kt TCs, compared to an expected 13-day disruption from wind exposure, cities issuing multi-level, multi-hazard warnings recovered by Day 4; under 64 kt or stronger TCs, recovery was reduced to Day 5 compared to the projected 21 days. In other words, when all warning types were issued, recovery times were shortened by 55.6 % under 34 kt TCs, increasing to 76.2 % under 64 kt or stronger TCs. Notably, cities that implemented multi-level, multi-hazard warnings also tended to issue stronger and earlier warnings at the same TC intensity. Given that both higher-intensity warnings and longer lead times are associated with faster recovery (Figs. 5c-5d, Supplementary Fig. S12), the observed acceleration likely reflects the joint influence of multiple warning types, stronger warning signals, and earlier warning issuance.

Despite the reduced exposure and shortened recovery time afforded by early warnings, cities were still affected by hazardous weather. Protected resilience was quantified to capture the residual impacts under such protection. As shown in Fig. 6, Chinese cities exhibited no significant differences in protected resilience when facing 34 kt or 50 kt TCs. However, under TCs of 64 kt or stronger, although early warnings substantially reduced direct exposure on the impact day and accelerated recovery, cities' protected resilience declined significantly (Fig. 6). In short, while preparatory actions mitigated part of the impact, TCs

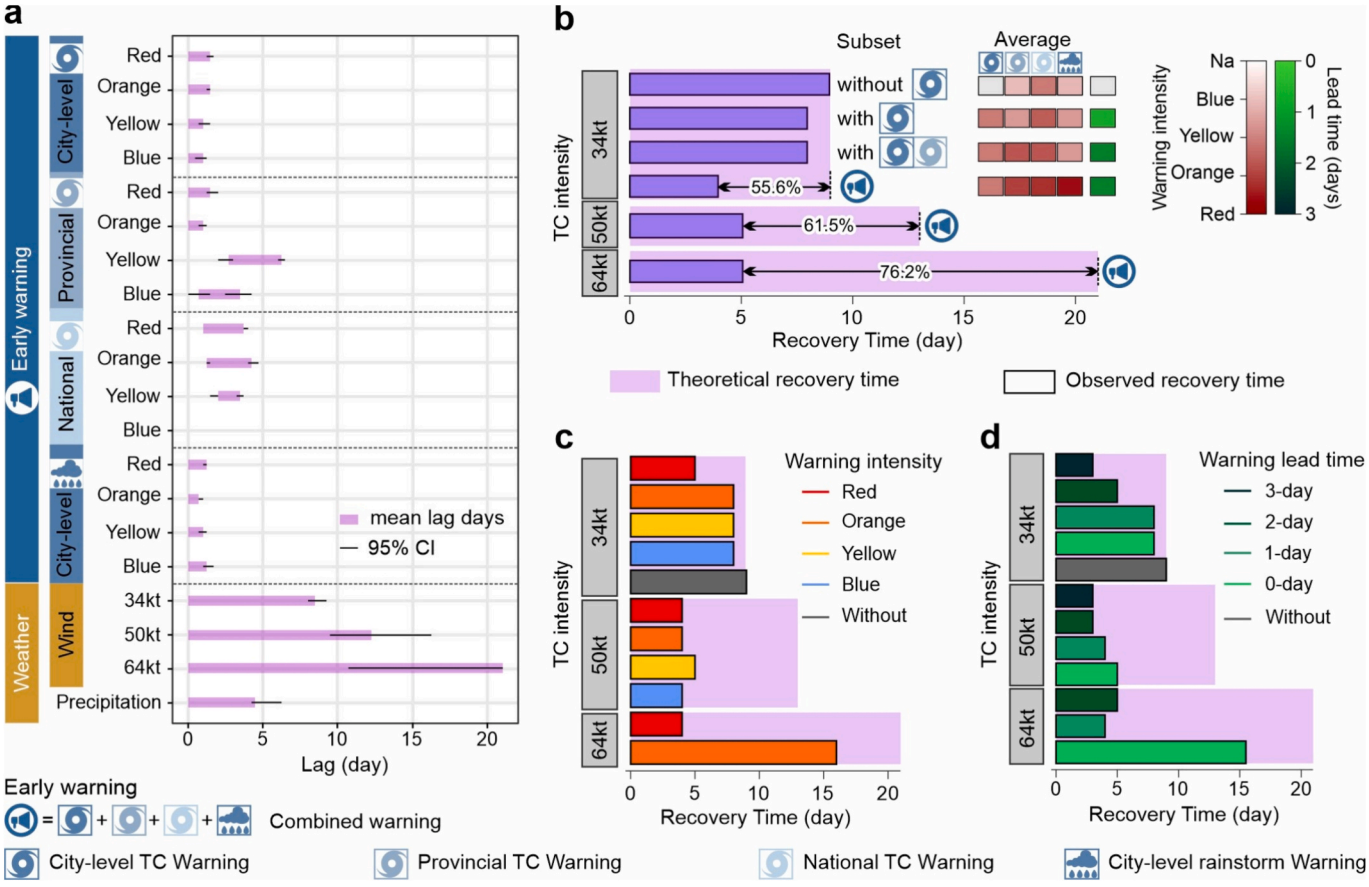



**Fig. 5. Recovery time after TCs. a**, Lag days (theoretical recovery time) of different warning and hazardous weather conditions on intracity mobility changes, with 95% confidence intervals (CIs); **b, c, d**, Average observed recovery times under varying TC intensities across different combinations of warning types issued during the event (**b**), city-level TC warning intensity levels (**c**), and lead times of warning issuance (**d**), with shaded areas indicating the mean TC lag periods presented in (**a**). All lead times are measured based on the lead time of city-level TC warnings.

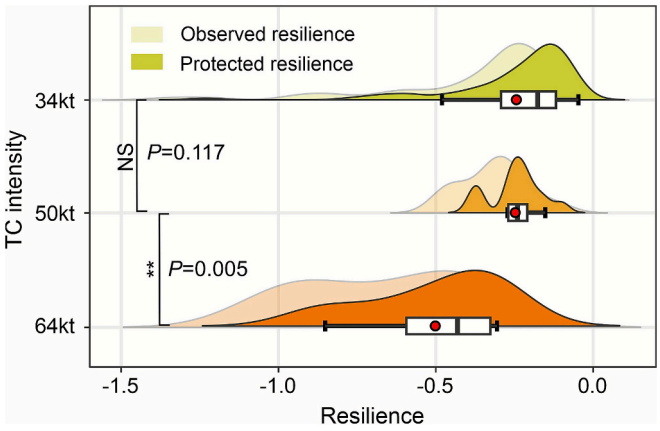



**Fig. 6. Protected resilience to TCs.** Half-violin plots display the data distributions, while boxplots present statistical summaries, where the central line represents the median and solid circles indicate the mean values. Significance levels were determined using two-sided Wilcoxon tests (*** P < 0.001; ** P < 0.01; * P < 0.05; NS, P > 0.05).

exceeding 64 kt imposed stresses beyond what cities' preparedness could fully absorb.

### 4.4. Variations in the benefits of early warnings across TC frequency, geographic locations, and socioeconomic conditions

The effectiveness of early warnings may vary across urban contexts. We found that early warnings were associated with significantly higher preemptive reduction ratios in high-frequency, coastal, and wealthier cities compared to low-frequency, inland, and less affluent ones on TC exposure days (Figs. 7a-7d). This disparity was related with stronger behavioural responses to equivalent warnings in high-exposure and coastal areas. For instance, under orange city-level TC warnings, high-frequency cities exhibited a 6.8 % reduction in intracity mobility intensity (95 % CI, 5.1 %–8.4 %) compared to 5.5 % (95 % CI, 1.5 %–9.4 %) in low-frequency cities, while coastal cities showed a 6.6 % reduction (95 % CI, 5.3 %–7.8 %) versus 2.4 % (95 % CI, 0–5.1 %) in inland cities. Notably, although less affluent cities exhibited greater mobility reductions per warning (Fig. 7c), they achieved a 21.6 % lower preemptive reduction ratio (46.4 % vs. 67.6 %) compared to wealthier cities, largely because many exposure days in less affluent cities lacked city-level TC warnings (Fig. 7d, Appendix Fig. A1). This difference points to unequal infrastructural capacity and underscores the importance of institutional preparedness.

Compared with single city-level TC warnings, the combination of multi-level and multi-hazard warnings was associated with substantially larger relative gains in avoided direct population exposure in low-frequency, inland, and less affluent cities (increases of 941.6 %, 380.8 %, and 62.7 %, respectively) (Fig. 7e). However, the absolute added benefits were greater in high-frequency, coastal, and wealthier cities (15.1 million, 13.8 million, and 8.7 million population-days, respectively) due to their larger baseline exposure. Therefore, from an absolute perspective, implementing MHEWS in high-frequency, coastal, and wealthier regions yields the largest direct benefits, while from a relative improvement perspective, low-frequency, inland, and less affluent areas achieve the greatest proportional gains.

Importantly, under the protection of MHEWS, protected resilience capacity did not differ significantly across cities by TC frequency or economic status. However, geographic location remained a significant factor, with coastal cities exhibiting significantly lower protected resilience than inland cities. While coastal cities achieved a median preemptive reduction ratio of 72.9 % (IQR, 55.2 %–95.2 %) on TC exposure days (Appendix Fig. A2), only 32.1 % (IQR, 16.5 %–46.2 %) of the total mobility reduction over the impact-to-recovery period could be associated with early warnings (Supplementary Fig. S13). This discrepancy highlights that despite strong anticipatory responses, coastal cities remain disproportionately vulnerable to the direct physical impacts of TCs.

### 4.5. Sensitivity analysis

Our main findings remained robust across a series of sensitivity analyses. To address potential uncertainties, we tested alternative wind modelling approaches (Supplementary Table S7, Appendix Fig. A3) and data from different time periods (2021 and 2022) (Supplementary Table S8, Appendix Fig. A4) (details in Methods). While specific numerical values varied slightly, the overall conclusion remained robust across all analyses, i.e., more than half of the mobility reduction during TCs was associated with preemptive actions triggered by early warnings. Importantly, with early warnings in place, no statistically significant difference in protected resilience was observed between 34 kt and 50 kt TC exposures.

## 5. Discussion

To the best of our knowledge, this study provides the first large-scale, behaviour-based quantification of how MHEWS shape disaster resilience under TC impacts, leveraging real-time mobility data from 1.1 billion mobile devices across 19 TC events in China. By disentangling the contributions of different warning types and levels, we provide empirical evidence of the combined and added benefits of MHEWSs in reducing population exposure, accelerating recovery, and shaping protected resilience to the impacts of extreme weather. The conceptual framework developed here is generalizable and can be adapted to assess early-warning effectiveness across these areas. As climate risks escalate globally, applying this dynamic, behaviour-based approach in diverse settings offers critical insights for designing context-specific MHEWS and strengthening global disaster preparedness.

Our findings highlight that early warnings are not merely supplementary to structural adaptation but are central to triggering anticipatory human behaviour. On TC exposure days, over half of the observed reductions in intracity mobility were associated with early warnings, avoiding an additional 54.4 % of direct exposure compared to city-level TC warnings alone. When multiple warning types were combined, average recovery durations shortened by 56–76 %, depending on TC intensity, underscoring the powerful combined effects of MHEWS. Notably, the largest absolute protective benefits accrued to high-frequency, coastal, and wealthier cities, while the greatest proportional gains were observed in low-frequency, inland, and less affluent regions. While severe disasters do not necessarily alter global policy frameworks (Nohrstedt et al., 2021), they shape local risk awareness (Riris et al., 2024) and warning effectiveness, helping ensure that cities frequently impacted by TCs are not more vulnerable than those low-frequency cities when protected by robust MHEWS. Such experience-driven awareness can also be cultivated through education and preparedness programs (UNDRR, 2023). Our empirical findings emphasize the importance of strengthening early-warning education and emergency drills in low-frequency and inland cities, as well as the urgency of improving the accuracy and coverage of early warnings in less affluent cities within China's MHEWS development.

Despite these benefits, our results reveal persistent disparities in warning issuance that can be mitigated by multi-level warning coverage. Although less affluent cities demonstrated strong per-warning behavioural responsiveness, they issued fewer warnings overall, leaving larger portions of their populations exposed. This suggests that infrastructural and institutional gaps, rather than differences in risk perception or behavioural capacity, are key drivers of inequitable protection. Such inequalities in disaster management across cities with differing economic conditions are widespread globally (Cutter & Finch, 2008; Ronco et al., 2023). As climate change intensifies TC hazards, failing to close

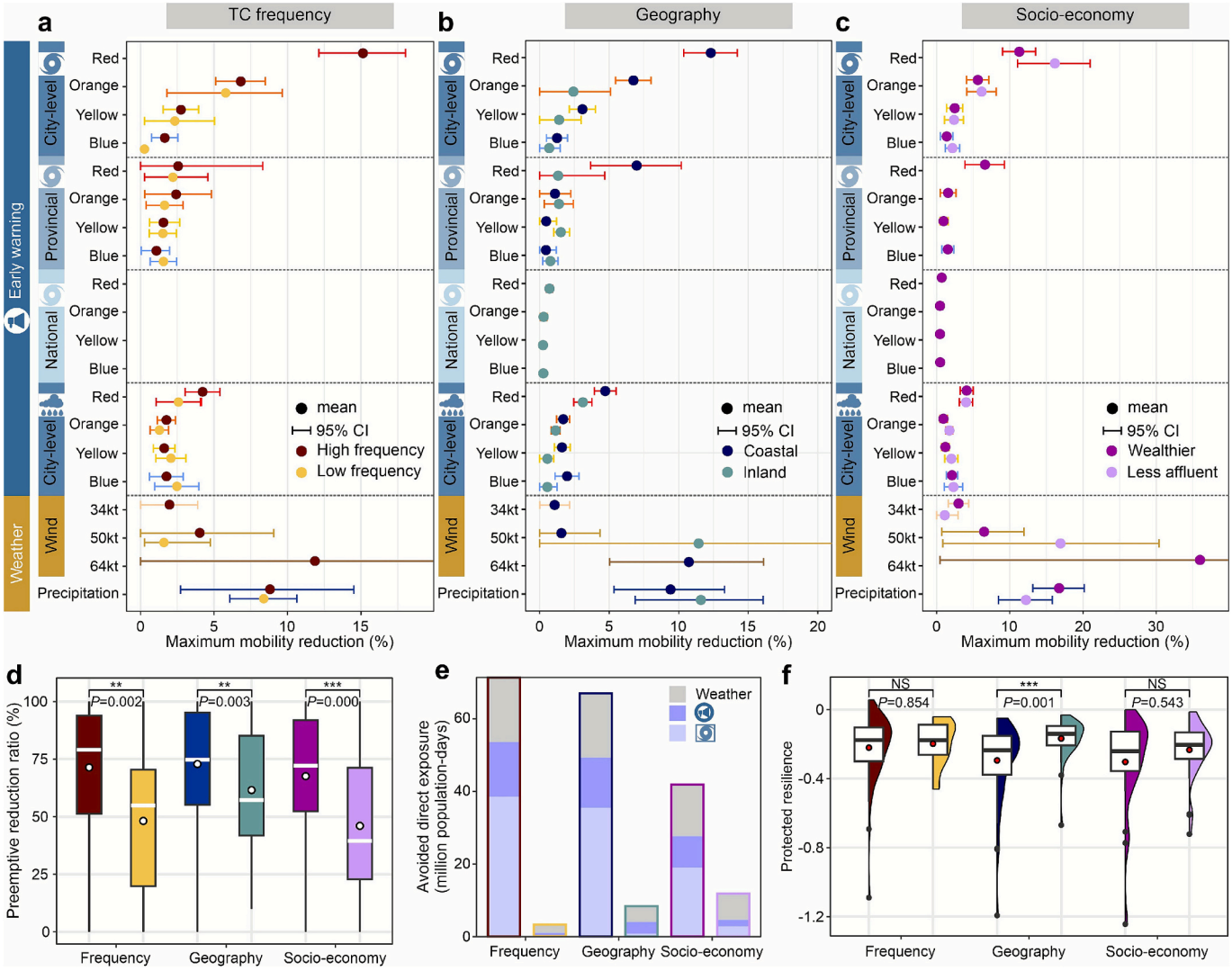



**Fig. 7. Variations in the effect of early warnings across cities with different TC frequencies, geographical locations, and socio-economic conditions.** The maximum mobility reductions and their 95 % CIs for different warnings and hazardous weather conditions are shown for cities with low-frequency and high-frequency TCs (**a**), coastal and inland cities (**b**), and wealthier and less affluent cities (**c**). The preemptive reduction ratio on TC exposure days (**d**), total avoided direct population exposure (**e**), and protected resilience at 34kt and 50kt TCs (**f**) across city groups were compared. Significance was determined using a two-sided Wilcoxon test (*** $P < 0.001$; ** $P < 0.01$; * $P < 0.05$; NS. $P >= 0.05$). The models' goodness-of-fit criteria are detailed in Supplementary Table S4-S6.

these institutional gaps risks exacerbating health and economic inequalities by increasing exposure in under-protected populations (Frankenberg et al., 2020). In China, the presence of multi-level and multi-hazard warnings has partly mitigated such inequalities by strengthening overall protective coverage, ensuring that under comparable TC intensities, less affluent cities did not exhibit significantly lower resilience than wealthier counterparts. This finding suggests that for countries, MHEWSs, compared with single-hazard EWSs, are not redundant but essential for ensuring equitable disaster preparedness.

Our analysis also underscores a widely recognized challenge: accurate early warning issuance does not automatically translate into preparatory behavioural responses. National-level TC warnings, provincial low-intensity TC warnings, and low-intensity city-level rainstorm warnings were not significantly associated with intracity mobility reductions. Prior studies have attributed such ineffectiveness to limited public understanding of warning messages or low trust in official information sources (Roy et al., 2015; Perera et al., 2020; Kitazawa & Hale, 2021; Yore & Walker, 2021). By linking our results with actionable guidance from China's official protocols (Appendix Table A1), we found that warnings accompanied by mandatory measures were markedly more effective in prompting preventive behaviour. This likely stems from China's centralized, top-down governance and communication system, where government-issued warnings are tied to coordinated and enforceable actions. A similar pattern was observed during TC Amphan (May 2020) in Bangladesh, where the involvement of security forces in organized evacuations enhanced compliance and effectiveness (Islam et al., 2021). Therefore, mandatory measures can be considered a viable policy instrument in centralized systems during their MHEWS design when an extreme hazard is around the corner.

Furthermore, we found that even under MHEWS protection, cities facing TCs at 64kt or above exhibited significantly lower protected resilience compared to those facing 34 kt or 50 kt storms. Coastal cities, in particular, demonstrated substantially lower protected resilience than inland cities when exposed to similar TC intensities. These findings reflect the limits of behavioural adaptation under extreme physical impacts: MHEWS alone cannot fully substitute for robust hard infrastructure, adaptive land-use planning, and compound flood management, especially in densely populated coastal zones. This underscores the need for integrated adaptation strategies that combine behavioural, institutional, and structural measures to comprehensively strengthen

resilience.

This study has several limitations. First, our analysis was conducted at the city-day scale using Baidu mobility data, which, although nationally representative, lack demographic detail and finer temporal resolution. Integrating multi-source and sub-daily mobility datasets from other platforms would allow for more granular spatiotemporal analyses and a deeper understanding of MHEWS impacts. Second, we treated warnings as independent events, which may have underestimated their effects by overlooking dependencies among warnings of different administrative levels, hazard types, and their interactions with hazard intensity. Sensitivity analyses confirmed that concurrent national- or provincial-level warnings enhanced the effectiveness of city-level TC warnings, particularly under high-intensity (red) conditions (Supplementary Fig. S14); the issuance of city-level TC warnings amplified the effectiveness of simultaneously released rainstorm warnings (Supplementary Fig. S15); and the same level of TC warning might exhibit different effects across diverse TC intensities (Supplementary Fig. S16). Future research could apply models capable of detecting complex interactions, such as random forest or Bayesian multilevel interaction models. Third, our analysis focused on China's centralized MHEWS framework, where residents are instructed to shelter in place and evacuations are centrally coordinated. In more decentralized systems, such as those in the United States and Japan, mobility changes may reflect both voluntary evacuation and stay-at-home behaviours (Yabe et al., 2020; Hong et al., 2021), complicating interpretation. Cross-national comparative analyses are therefore needed in the future to capture institutional diversity. Finally, our focus on mobility-based resilience provides a useful proxy for behavioural and functional recovery, yet it captures only one facet of overall resilience. A comprehensive assessment of MHEWS benefits requires broader consideration of economic, infrastructural, and health dimensions that underpin long-term adaptive capacity.

This study demonstrates that MHEWSs shape disaster resilience by reducing exposure, accelerating recovery, and narrowing protected resilience gaps across diverse urban contexts. Our findings provide empirical guidance for optimizing MHEWS architectures and reinforce their critical role in climate adaptation strategies. As climate risks intensify, ensuring universal, multi-layered, and locally tailored MHEWS coverage will be essential not only for minimizing disaster impacts but also for advancing equitable and sustainable development worldwide.

## 6. Code availability

The codes used in the study are available at: https://github.com/fionaliuhy/TC-early-warning.

The authors used a generative AI tool (Gemini Pro 2.5) for grammar checking.

## CRediT authorship contribution statement

**Haiyan Liu:** Writing – review & editing, Writing – original draft, Visualization, Validation, Supervision, Methodology, Conceptualization. **Jianghao Wang:** Writing – review & editing, Validation, Supervision, Formal analysis, Conceptualization. **Zhifeng Cheng:** Writing – review & editing, Validation, Methodology. **Siqin Wang:** Writing – review & editing, Validation, Investigation, Conceptualization. **Laurence Hawker:** Writing – review & editing, Supervision, Formal analysis. **Jiatong Han:** Writing – review & editing. **Phil J. Ashworth:** Writing – review & editing. **Steve Darby:** Writing – review & editing. **Faith Ka Shun Chan:** Writing – review & editing. **Jian Liu:** Writing – review & editing. **Andrew J. Tatem:** Writing – review & editing, Supervision, Funding acquisition, Conceptualization. **Shengjie Lai:** Writing – review & editing, Validation, Supervision, Methodology, Conceptualization.

## Declaration of competing interest

The authors declare that they have no known competing financial interests or personal relationships that could have appeared to influence the work reported in this paper.

## Acknowledgements

We thank Baidu and other data providers for sharing the openly available datasets. This work was supported by the National Natural Science Foundation of China (42222110, 42571540, W2432029), the National Institute for Health (MIDAS Mobility R01AI160780), the UKRI Natural Environment Research Council (EvoFlood NE/S015817/1), the Southern Marine Science and Engineering Guangdong Laboratory (Zhuhai) (SML2022SP401 and SML2021SP102), and open grant from the LREIS, Chinese Academy of Sciences. The funders had no role in the conceptualization, design, data collection, analysis, publication decision, or manuscript preparation. A large language model (specifically, Gemini Pro 2.5) was used for grammar checking.

## Appendix

.

**Table A1**
**The triggering weather conditions and official actionable guidance corresponding to early warnings at the city-level in China.** All actionable guidance for high-intensity warnings are additional to those implemented for lower-intensity ones.

| Targeted Hazard | Intensity | Triggering Weather Conditions | | Actionable Guidance | |
|---|---|---|---|---|---|
| | | Weather conditions | Lead time | Actionable guidance | With mandatory measures |
| TC (Typhoon) | Blue | Possible or ongoing TC winds below 34 kt | 24 h | 1. Government prepares for the typhoon. 2. Suspend outdoor and high-altitude work. 3. Vessels return to port or reroute. 4. Secure structures, cut off hazardous power supplies. | No |
| | Orange | Possible or ongoing TC winds 34–50 kt | 24 h | 1. Suspend large indoor/outdoor gatherings. 2. Nurseries, kindergartens, and primary/secondary schools suspend classes. | Yes |
| | Yellow | Possible or ongoing TC winds 50–64 kt | 12 h | 1. All schools suspend classes. | Yes |
| | Red | Possible or ongoing TC winds over 64 kt | 6 h | 1. Suspend gatherings, classes, and business operations (except essential industries). | Yes |
| Rainstorm | Blue | Rainfall expected to reach or exceed 50 mm | 12 h | 1. Government prepares. 2. Drivers exercise caution. | No |

(*continued on next page*)

**Table A1** (*continued*)

| Targeted Hazard | Intensity | Triggering Weather Conditions | | Actionable Guidance | |
|---|---|---|---|---|---|
| | | Weather conditions | Lead time | Actionable guidance | With mandatory measures |
| | Orange | Rainfall expected to reach or exceed 50 mm | 6 h | 1. Traffic control in flooded areas. 2. Cut power, halt outdoor work, relocate people. | No |
| | Yellow | Rainfall expected to reach or exceed 50 mm | 3 h | 1. Schools and workplaces in danger zones should close. | No |
| | Red | Rainfall expected to reach or exceed 100 mm | 3 h | 1. Suspend gatherings, and classes (except essential services). | Yes |

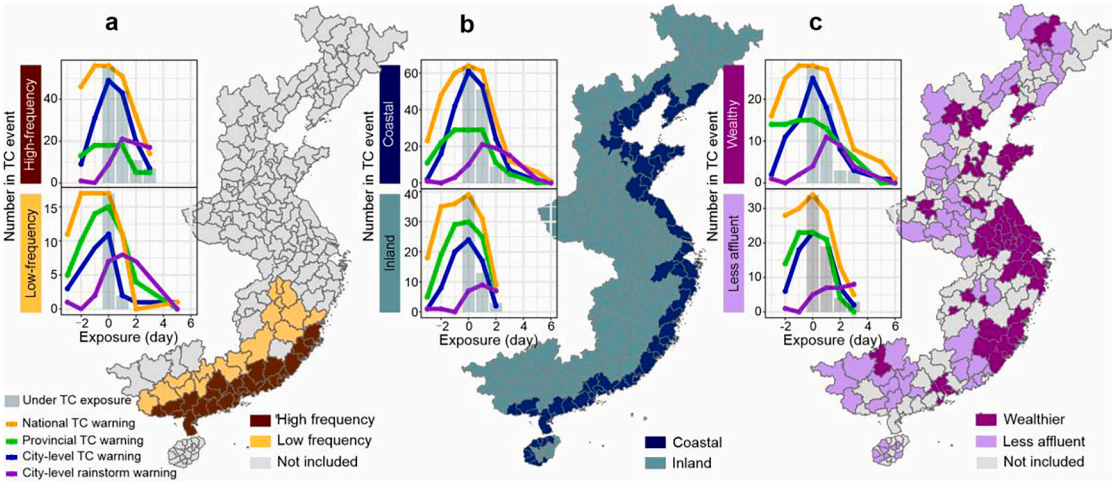



**Fig. A1.** Locations of different types of cities and their early warning issuance. The figure shows the geographic distribution and warning issuance patterns for various city types: a displays high-frequency (n = 28) and low-frequency cities (n = 16), b shows coastal (n = 62) and inland (n = 122) cities, and c depicts wealthier (n = 55) and less affluent (n = 54) cities. The warning issuance data records the number of different types of warnings issued before and after TC exposure for all events experienced by cities in each category in 2023.

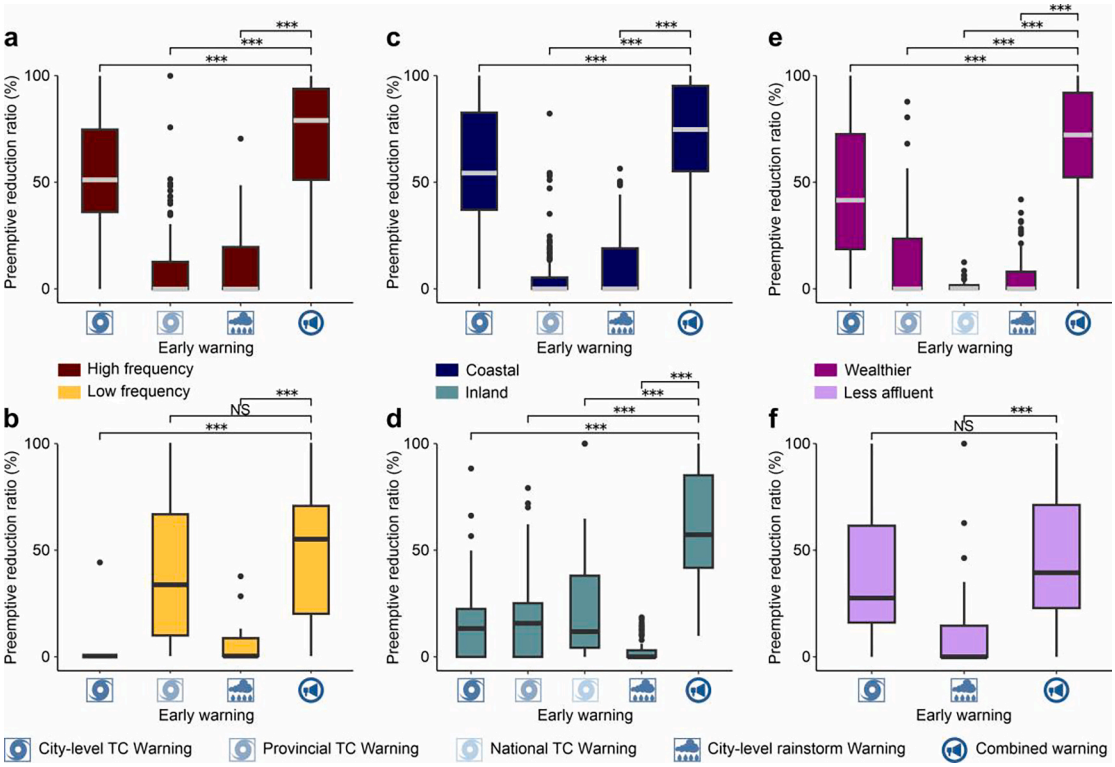



**Fig. A2.** Preemptive mobility reduction ratios on TC exposure days across different types of cities. a, b show results for high-frequency and low-frequency cities, c, d for coastal and inland cities, and e, f for wealthier and less affluent cities. Boxplots present the statistical summaries, with significance determined using a two-sided Wilcoxon test (*** P < 0.001; ** P < 0.01; * P < 0.05; NS. P >= 0.05).

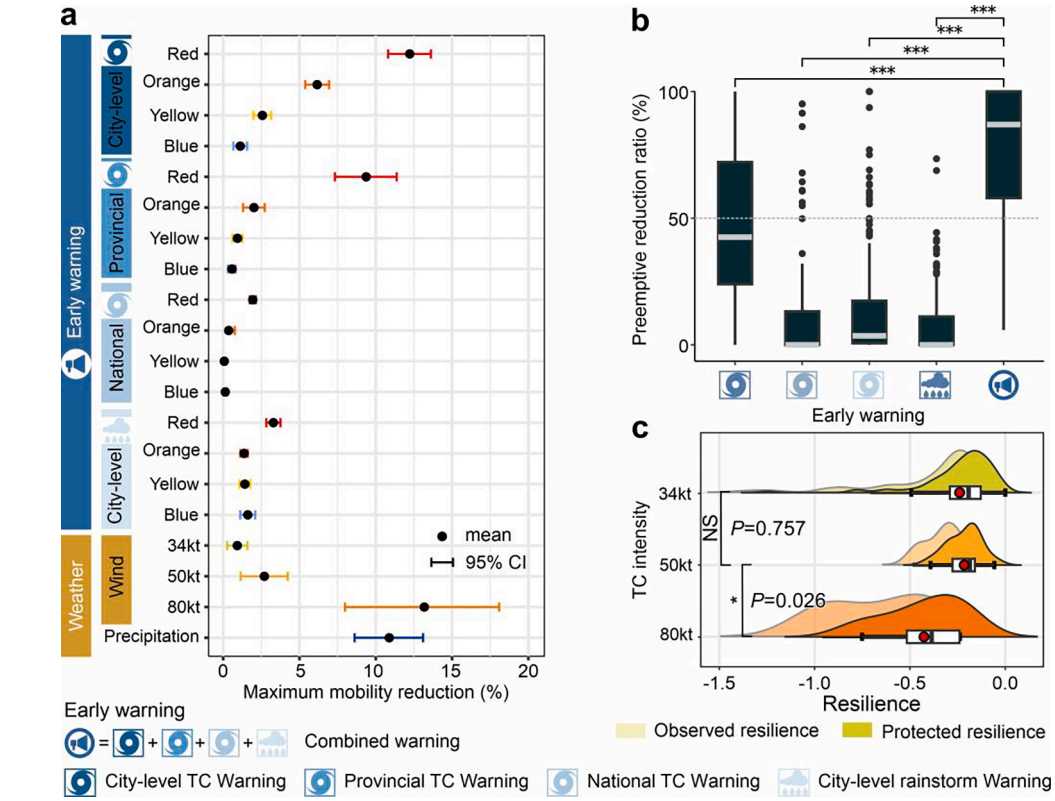



**Fig. A3.** Impact of warnings on intracity mobility resilience during TC exposure, calculated based on the Holland wind model. a, Maximum mobility reduction and its 95 % confidence interval for intracity mobility under different warnings and hazardous weather conditions. b, Preemptive reduction ratios for various warnings on TC exposure days, considering a 3-day warning lead-time. c, Mobility observed and protected resilience capacity at varying TC intensity. All data are presented in the same manner as in Fig. 2 and Fig. 4. Significance was determined using a two-sided Wilcoxon test (*** P < 0.001; ** P < 0.01; * P < 0.05; NS. P >= 0.05). The model's goodness-of-fit criteria are detailed in S7.

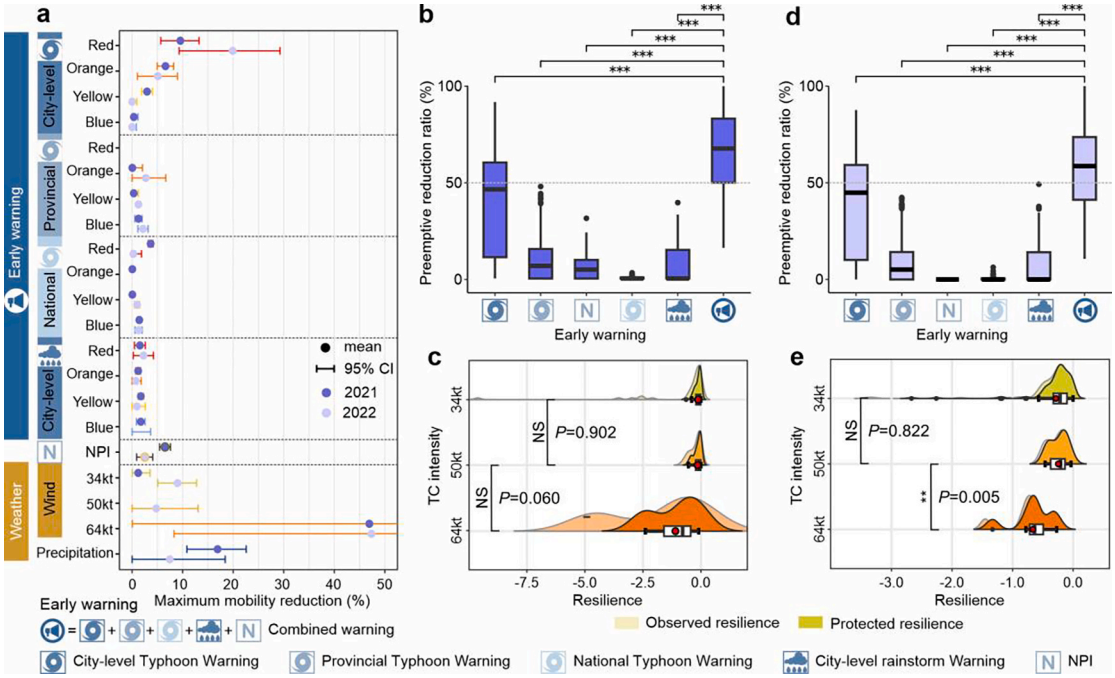



**Fig. A4.** Impact of warnings on intracity mobility resilience in 2021 and 2022. a, Maximum mobility reduction and its 95 % confidence interval for intracity mobility under different warnings and hazardous weather conditions. b, d, Preemptive reduction ratios for various warnings on TC exposure days, considering a 3-day warning lead time. c, e, c, Mobility observed resilience and protected resilience capacity at varying TC intensity. All data are presented in the same manner as in Fig. 2 and Fig. 4. Significance was determined using a two-sided Wilcoxon test (*** P < 0.001; ** P < 0.01; * P < 0.05; NS. P >= 0.05). b and c show the results for 2021, while d and e show the results for 2022. The model's goodness-of-fit criteria are provided in S8.

## Data availability

All datasets used in this study are publicly available from open-access repositories or official platforms. Tropical cyclone track data were obtained from the China Meteorological Administration (CMA) (https://typhoon.nmc.cn/web.html). Human mobility data were retrieved from Baidu Qianxi data portal (https://qianxi.baidu.com/). Early warning data were collected from the National Emergency Broadcast (https://www.cneb.gov.cn/), the official multi-channel network (MCN) account of the China National Early Warning Information Release Center, and verified local meteorological bureau Weibo accounts. Meteorological data were obtained from ERA5-Land (https://cds.climate.copernicus.eu/). Population data were sourced from WorldPop (https://www.worldpop.org/). Administrative boundaries were accessed via the Amap API (https://datav.aliyun.com/portal/). Socioeconomic and holiday data were derived from provincial/city statistical yearbooks and the official website of the General Office of the State Council of China. COVID-19 stringency index data were obtained from the Oxford COVID-19 Government Response Tracker (https://www.bsg.ox.ac.uk/research/covid-19-government-response-tracker). Researchers may contact the corresponding author for any inquiries regarding data access or clarification.

## References


WMO. Atlas of Mortality and Economic Losses from Weather, Climate and Water Extremes (1970–2019). *Geneva* (2021).

Peduzzi, P., et al., 2012. Global trends in tropical cyclone risk. Nat. Clim. Chang. 2, 289–294.

IPCC. Climate Change 2022: Impacts, Adaptation, and Vulnerability (eds Pörtner, H.-O. et al.) *Cambridge Univ. Press* (2022).

Jing, R. et al. Global population profile of tropical cyclone exposure from 2002 to 2019. *Nature*, doi:10.1038/s41586-023-06963-z (2023).

UNDRR. Forensic Insights for Future Resilience, Learning from Past Disasters. *Geneva* (2024).

Tennant, E., Gilmore, E.A., 2020. Government effectiveness and institutions as determinants of tropical cyclone mortality. PNAS 117, 28692–28699.

UNDRR. Global Status of Multi-Hazard early-warning Systems. *Geneva* (2023).

United Nations. Sendai Framework for Disaster Risk Reduction 2015 - 2030. *Sendai* (2015a).

Fearnley, A.C.T.C.J., 2023. Disaster early-warning systems can succeed — but collective action is needed. Nature 623, 478–482.

Fundel, V.J., Fleischhut, N., Herzog, S.M., Göber, M., Hagedorn, R., 2019. Promoting the use of probabilistic weather forecasts through a dialogue between scientists, developers and end-users. Q. J. R. Meteorol. Soc. 145, 210–231.

State Council Disaster Investigation Team, P. R. China. Investigation Report on July 20 extremely heavy rainstorm Disaster in Zhengzhou, Henan Province. http://www.mem.gov.cn/gk/sgcc/tbzdsgdcbg/202201/P020220121639049697767.pdf (2022).

Terrill, M. Lessons from Helene: ASU professors explain the complexities behind emergency management. https://news.asu.edu/20241003-environment-and-sustainability-lessons-helene-asu-professors-explain-complexities-behind (2024).

Cremen, G., Galasso, C., Zuccolo, E., 2022. Investigating the potential effectiveness of earthquake early-warning across Europe. Nat. Commun. 13, 639.

Roy, C., Sarkar, S. K., Åberg, j., and Kovordanyi, R. The Current Cyclone Early Warning System in Bangladesh: Providers' and Receivers' Views. *Int. J. Disast. Risk Re.* 12: 285–99 (2015).

Perera, C., Jayasooriya, D., Jayasiri, G., et al., 2020. Evaluation of gaps in early warning mechanisms and evacuation procedures for coastal communities in Sri Lanka. Int. J. Disaster Resil. Built Environ. 11 (3), 415–433.

Kitazawa, K., Hale, S.A., 2021. Social media and early warning systems for natural disasters: a case study of typhoon Etau in Japan. Int. J. Disast. Risk Re. 52, 101926.

Yore, R., Walker, J.F., 2021. Early warning systems and evacuation: rare and extreme versus frequent and small-scale tropical cyclones in the Philippines and Dominica. Disasters 45 (3), 691–716.

Fekete, A., Sandholz, S., 2021. Here comes the flood, but not failure? lessons to learn after the heavy rain and pluvial floods in Germany 2021. Water 13.

Dittmer, C., Lorenz, D.F., 2024. Emergent, extending, expanding and established citizen disaster response in the German Ahr valley flood in 2021. Int. J. Disast. Risk Re. 105.

Yabe, T., Rao, P.S.C., Ukkusuri, S.V., Cutter, S.L., 2022. Toward data-driven, dynamical complex systems approaches to disaster resilience. PNAS 119.

Liu, Y., et al., 2023a. Quantifying human mobility resilience to the COVID-19 pandemic: a case study of Beijing, China. Sustain. Cities Soc. 89.

Hatchett, B.J., Bnemarhnia, T., Guirguis, K., et al., 2021. Mobility data to aid assessment of human responses to extreme environmental conditions. Lancet Planet. Heath 5 (10), E665–E667.

Lu, X., Bengtsson, L., Holme, P., 2012. Predictability of population displacement after the 2010 Haiti earthquake. PNAS 109 (29), 11576–11581.

Wilson, R., et al., 2016. Rapid and near real-time assessments of population displacement using mobile phone data following disasters: the 2015 Nepal Earthquake. PLoS Curr 8.

Liu, H., et al., 2023b. Combined and delayed impacts of epidemics and extreme weather on urban mobility recovery. Sustain. Cities Soc. 99.

Acosta, R.J., Kishore, N., Irizarry, R.A., Buckee, C.O., 2020. Quantifying the dynamics of migration after hurricane maria in Puerto Rico. PNAS 117 (51), 32772–32778.

Deng, H., Aldrich, D.P., Danziger, M.M., 2021. High-resolution human mobility data reveal race and wealth disparities in disaster evacuation patterns. Humanit. Soc. Sci. Commun. 8 (1), 1–8.

United Nations, 2015b. Transforming Our World: The 2030 Agenda for Sustainable Development. https://www.un.org/ohrlls/sites/www.un.org.ohrlls/files/2030_agenda_for_sustainable_development_web.pdf.

Wang, J., Hu, Y., 2024. Unraveling hurricane ian's impact: a multiscale analysis of mobility networks in Florida. Transp. Res. D Transp. Environ. 136 (104482), 104482.

Tang, J., et al., 2023. Resilience patterns of human mobility in response to extreme urban floods. Nat. Sci. Rev. 10.

Qian, J., et al., 2024. Measuring community resilience inequality to inland flooding using location aware big data. Cities 149, 104915.

Abad, R.P., Fillone, A.M., 2020. Changes in travel behavior during flood events in relation to transport modes: the Case of Metro Manila, Philippines. Transp. Res. Procedia 48, 1592–1604.

Lu, X., et al., 2016. Unveiling hidden migration and mobility patterns in climate stressed regions: a longitudinal study of six million anonymous mobile phone users in Bangladesh. Global Environ. Chang. 38, 1–7.

Yabe, T., Tsubouchi, K., Fujiwara, N., Sekimoto, Y., Ukkusuri, S.V., 2020. Understanding post-disaster population recovery patterns. J. R. Soc. Interface 17 (163), 20190532.

Wilkinson, E., Fernandez, A. C., and Quevedo, A. Special Report on Human Mobility and Disaster Risk in Latin America and the Caribbean. United Nations Office for Disaster Risk Reduction (UNDRR), Geneva. https://www.developmentaid.org/api/frontend/cms/file/2024/07/ENG-ANNEX-RAR21-Special-Report-on-Human-Mobility-and-Disaster-Risk-in-Latin-America-and-the-Caribbean.pdf (2024).

Haque, U., et al., 2012. Reduced death rates from cyclones in Bangladesh: what more needs to be done? B. World Health Organ. 90, 150–156.

Zhang, X., Li, N., 2022. Characterizing individual mobility perturbations in cities during extreme weather events. Int. J. Disast. Risk Re. 72, 102849.

CRED. EM-DAT: The International Disaster Database. Université Catholique de Louvain, Brussels, Belgium. https://www.emdat.be (2025).

Office of the National Disaster Reduction Committee & Ministry of Emergency Management. 2024 National Natural Disaster Summary of China https://www.gov.cn/lianbo/bumen/202501/content_6999765.htm (2025).

State Council. National emergency management system plan during the 14th five-year plan period. Ministry of Emergency Management of China. https://www.mem.gov.cn/zl/202208/P020220823583813558584.pdf (2022).

Gibbs, H., Liu, Y., Pearson, C.A.B., et al., 2020. Changing travel patterns in China during the early stages of the COVID-19 pandemic. Nat. Commun. 11, 5012.

Hong, B., Bonczak, B.J., Gupta, A., Kontokosta, C.E., 2021. Measuring inequality in community resilience to natural disasters using large-scale mobility data. Nat. Commun. 12.

Google LLC. COVID-19 Community Mobility Reports. https://www.google.com/covid19/mobility/ (2022).

Holland, G.J., Belanger, J.I., Fritz, A., 2010. A revised model for radial profiles of hurricane winds. Mon. Weather Rev. 138, 4393–4401.

Feng, J., et al., 2014. An overview of the china meteorological administration tropical cyclone database. J. Atmos. Ocean. Tech. 31, 287–301.

Chavas, D.R., Knaff, J.A., 2022. A simple model for predicting the tropical cyclone radius of maximum wind from outer size. Weather Forecast. 37, 563–579.

Lin, N., Chavas, D., 2012. On hurricane parametric wind and applications in storm surge modeling. J. Geophys. Res.-Atmos. 117.

Holland, G.J., 1980. An analytic model of the wind and pressure profiles in hurricanes. Mon. Wea. Rev. 108, 1212–1218.

Xiao, Y.F., et al., 2011. Typhoon wind hazard analysis for southeast China coastal regions. Struct. Saf. 33, 286–295.

Stevens, F.R., Gaughan, A.E., Linard, C., Tatem, A.J., 2015. Disaggregating census data for population mapping using random forests with remotely-sensed and ancillary data. PLoS One 10, e0107042.

Hersbach, H., et al., 2020. The ERA5 global reanalysis. Q. J. Roy. Meteor. Soc. 146, 1999–2049.

Lai, S., et al., 2022. Global holiday datasets for understanding seasonal human mobility and population dynamics. Sci. Data 9, 17.

Hale, T., et al., 2021. A global panel database of pandemic policies (Oxford COVID-19 Government Response Tracker). Nat. Hum. Behav. 5, 529–538.

Banerjee, S., Carlin, B.P., Gelfand, A.E., 2014. Hierarchical Modeling and Analysis for Spatial Data, 2nd ed. Chapman and Hall/CRC, Boca Raton, FL.

Lowe, R., et al., 2021. Combined effects of hydrometeorological hazards and urbanisation on dengue risk in Brazil: a spatiotemporal modelling study. Lancet Planet. Health 5, e209–e219.

Simpson, D., Rue, H., Riebler, A., Martins, T.G., Sørbye, S.H., 2017. Penalising model component complexity: a principled, practical approach to constructing priors. Stat. Sci. 32 (1), 1–28.

Blangiardo, M., Cameletti, M., Baio, G., Rue, H., 2013. Spatial and spatio-temporal models with R-INLA. Spat. Spatiotemporal Epidemiol. 7, 39–55.

Ding, S., et al., 2024. Understanding the spatial disparity in socio-economic recovery of coastal communities following typhoon disasters. Sci. Total Environ. 919, 170831.

Gasparrini, A., Armstrong, B., Kenward, M.G., 2010. Distributed lag non-linear models. Stat. Med. 29, 2224–2234.
Huang, W., Li, S., Vogt;, T., et al., 2023. Global short-term mortality risk and burden associated with tropical cyclones from 1980 to 2019: a multi-country time-series study. Lancet Planet. Health 7 (8), e694–e705.
Fletcher, C., Moirano, G., Alcayna, T., et al., 2025. Compound and cascading effects of climatic extremes on dengue outbreak risk in the caribbean: an impact-based modelling framework with long-lag and short-lag interactions. Lancet Planet. Health 9 (8), 101279.
Zhao, Y., Gao, Y., 2024. Spatial patterns and trends of inter-city population mobility in China—based on Baidu migration big data. Cities 151, 105124.
Meta. Movement distribution. https://data.humdata.org/dataset/movement-distribution (2025).
Nohrstedt, D., Mazzoleni, M., Parker, C.F., Di Baldassarre, G., 2021. Exposure to natural hazard events unassociated with policy change for improved disaster risk reduction. Nat. Commun. 12.
Riris, P., et al., 2024. Frequent disturbances enhanced the resilience of past human populations. Nature 629, 837–842.
Cutter, S.L., Finch, C., 2008. Temporal and spatial changes in social vulnerability to natural hazards. PNAS 105, 2301–2306.
Ronco, M., et al., 2023. Exploring interactions between socioeconomic context and natural hazards on human population displacement. Nat. Commun. 14. https://doi.org/10.1038/s41467-023-43809-8.
Frankenberg, E., Sumantri, C., Thomas, D., 2020. Effects of a natural disaster on mortality risks over the longer term. Nat. Sustain. 3, 614–619.
Islam, M.T., Charlesworth, M., Aurangojeb, M., et al., 2021. Revisiting disaster preparedness in coastal communities since 1970s in Bangladesh with an emphasis on the case of tropical cyclone Amphan in May 2020. Int. J. Disast. Risk Re. 58 (102175), 102175.